



# Metamorphosis shapes cranial diversity and rate of evolution in salamanders

Anne-Claire Fabre<sup>1</sup>✉, Carla Bardua<sup>1,2</sup>, Margot Bon<sup>1</sup>, Julien Clavel<sup>1,3</sup>, Ryan N. Felice<sup>4</sup>, Jeffrey W. Streicher<sup>1</sup>, Jeanne Bonnel<sup>2</sup>, Edward L. Stanley<sup>5</sup>, David C. Blackburn<sup>5</sup> and Anjali Goswami<sup>1</sup>

**Metamorphosis is widespread across the animal kingdom and induces fundamental changes in the morphology, habitat and resources used by an organism during its lifetime. Metamorphic species are likely to experience more dynamic selective pressures through ontogeny compared with species with single-phase life cycles, which may drive divergent evolutionary dynamics. Here, we reconstruct the cranial evolution of the salamander using geometric morphometric data from 148 species spanning the order's full phylogenetic, developmental and ecological diversity. We demonstrate that life cycle influences cranial shape diversity and rate of evolution. Shifts in the rate of cranial evolution are consistently associated with transitions from biphasic to either direct-developing or paedomorphic life cycle strategies. Direct-developers exhibit the slowest rates of evolution and the lowest disparity, and paedomorphic species the highest. Species undergoing complete metamorphosis (biphasic and direct-developing) exhibit greater cranial modularity (evolutionary independence among regions) than do paedomorphic species, which undergo differential metamorphosis. Biphasic and direct-developing species also display elevated disparity relative to the evolutionary rate for bones associated with feeding, whereas this is not the case for paedomorphic species. Metamorphosis has profoundly influenced salamander cranial evolution, requiring greater autonomy of cranial elements and facilitating the rapid evolution of regions that are remodelled through ontogeny. Rather than compounding functional constraints on variation, metamorphosis seems to have promoted the morphological evolution of salamanders over 180 million years, which may explain the ubiquity of this complex life cycle strategy across disparate organisms.**

Developmental processes play a fundamental role in structuring the morphological diversity of organisms<sup>1–3</sup>, being both a driver of and a constraint on phenotypic change<sup>1,4,5</sup>. As such, shifts in development and life history can have profound impacts on the evolutionary trajectories of lineages. Early attempts to delineate these effects resulted in the recapitulationist doctrine, stating that ontogeny replicates phylogeny<sup>6</sup>. However, studies of groups such as amphibians have shown that shifts in developmental strategies (for example, biphasic development, direct development, paedomorphy and viviparity) have occurred many times. In some cases, metamorphic species can even eliminate later ontogenetic stages and mature with larval characteristics (a form of paedomorphosis), demonstrating that the relationship between ontogenetic and evolutionary dynamics is often complicated<sup>7</sup>. Biphasic development with a complex life cycle is a common developmental strategy<sup>8</sup> and has resulted in much of the exceptional diversity that is evident today (the majority of all animals, with most of the successful and speciose groups of insects (over 80%) and vertebrates (~50%); for example, see refs. <sup>8–14</sup>). This distribution indicates that metamorphosis may be an important driver of biodiversity overall, but why? Previous studies have suggested that larval stages may not overlap in resource use with adults<sup>15</sup>, meaning that intraspecific competition between larvae and adults is reduced. This may favour population growth, but it does not necessarily translate into phenotypic diversity<sup>16</sup>. Importantly, biphasic species typically undergo a change in environment alongside metamorphosis from the larval to the adult stage, which is coupled with

distinct physiological, morphological and functional changes. Such complex life cycles offer a conceptual framework to test the capacity of organisms to cope with environmental changes by producing morphological variation during their lifespan<sup>17,18</sup>.

One way for a lineage to evolve extreme phenotypic modifications is by having aspects of its morphology vary independently from other aspects (also defined as modularity), allowing each module (a quasi-autonomous subset of highly correlated traits) to vary and evolve independently. This modularity may increase the overall capacity of a species to generate heritable morphological variation and novel forms as well as potentially facilitating greater morphological diversification<sup>19,20</sup>. Life cycle complexity offers a unique perspective on these fundamental biological concepts, as radical transitions in form occur at multiple ontogenetic and evolutionary scales<sup>18</sup>. For example, the existence of a modular life cycle with compartmentalized developmental stages has led researchers to suggest the adaptive decoupling hypothesis<sup>21–24</sup>, where antagonistic selection pressures occur at each life-history stage, maintaining low genetic correlations between larval and adult traits. However, if the stages are not autonomous, structures that are required for different functions at different ontogenetic stages could be constrained in terms of their morphological evolution<sup>25</sup>. Metamorphosis may thus either increase developmental canalization, leading to reduced morphological diversity in metamorphic forms, or reset the pattern of variation between larval and adult stages and allow greater morphological diversity across species<sup>26</sup>.

<sup>1</sup>Department of Life Sciences, The Natural History Museum, London, UK. <sup>2</sup>Department of Genetics, Evolution and Environment, University College London, London, UK. <sup>3</sup>Univ Lyon, Université Claude Bernard Lyon 1, CNRS, ENTPE, UMR 5023 LEHNA, Villeurbanne, France. <sup>4</sup>Centre for Integrative Anatomy, Department of Cell and Developmental Biology, University College London, London, UK. <sup>5</sup>Florida Museum of Natural History, University of Florida, Gainesville, FL, USA. ✉e-mail: [a.fabre@nhm.ac.uk](mailto:a.fabre@nhm.ac.uk)

Among the organisms experiencing metamorphosis, salamanders (Amphibia: Caudata, ~ 700 species<sup>27,28</sup>) display a tremendous diversity of species, ecologies and life cycles with multiple independent evolutions thereof<sup>25,29–33</sup>. Salamanders therefore provide an excellent framework to study how developmental processes can produce morphological diversity. Interestingly, contrasting results have been found for salamanders depending on the morphological structure of interest. Bonett and Blair<sup>25</sup> found accelerated rates of body form and vertebral column evolution in species with simple life cycles (paedomorphic, aquatic species and direct-developing, terrestrial species). They also found that constraints on body form evolution are stage specific and that shifts in life cycle complexity can alter the dynamics of morphological evolution in salamanders. Ledbetter and Bonett<sup>33</sup> showed that limbs evolve faster and are less constrained for aquatic species (mostly paedomorphic) than for terrestrial species (mostly direct-developing). Vučić et al.<sup>26</sup> demonstrated that metamorphosis cannot be regarded as a developmental constraint on the overall external head in a newt. Finally, Blankers et al.<sup>34</sup> hypothesized that developmental constraints on phenotype may limit morphological evolution to different microhabitats in plethodontids on the basis of an analysis of body and appendage lengths.

Here, we assess the role of metamorphosis and the associated changes of environment in the evolution of morphological diversity and evolutionary modularity of the skull across salamanders displaying a diversity of life cycles. To do so, we generated a novel dataset describing cranial shape in salamanders at unprecedented scales, spanning the full phylogenetic, ecological and developmental breadth of Caudata, with species belonging to all families and representing nearly all genus-level diversity (>95% of extant genera; Fig. 1, Extended Data Figs. 1–3 and Supplementary Figs. 1–3). Changes in salamander skull shape during metamorphosis relate to changes in both diet and environment<sup>35</sup>, with musculoskeletal (bone and muscle) remodelling leading to the modification of certain bones (mostly bones involved in food processing, including the pterygoid and vomer), while other bones disappear entirely (such as the palatine portion of the palatopterygoid) or first appear after metamorphosis (such as the maxilla or the prefrontal)<sup>29,36</sup>. Consequently, assessing every cranial element is critical for uncovering the complexity of salamander cranial evolution. We test the prediction that adult phenotypes in biphasic and direct-developing species have lower disparities and evolutionary rates than those in paedomorphic species, as developmental canalization has been hypothesized to constrain developmental processes during metamorphosis<sup>26</sup>. In addition, we investigate whether the complexity of the life cycle or the extent of metamorphosis influence evolutionary modularity. Specifically, we hypothesize that biphasic species transitioning between environments and diets may exhibit increased fragmentation of phenotypic traits into evolutionary modules, compared with direct-developing and paedomorphic species experiencing just one environment. Alternatively, we hypothesize that species undergoing complete metamorphosis (biphasic and direct-developing species) may display more modular evolution than those experiencing no or differential metamorphosis (paedomorphic species). Finally, we explore the relationship between evolutionary rates and morphological variation for each cranial bone depending on life cycle. We predict that bones involved in food processing or those remodelled during metamorphosis have an elevated morphological diversity and rate of evolution and thus an increased ability to evolve.

## Results

**Life cycle and associated habitat differentiates adult cranial morphology.** There is a significant but low impact of size (centroid size) on salamander cranial shape evolution (phylogenetic generalized least squares,  $R^2=0.063$ ,  $P=0.001$ ; Supplementary Table 1 and Supplementary Fig. 4). The adult cranial morphological space (morphospace) of all 148 species can be summarized by 32 principal

components (PC) (and 42 phylogenetic PCs) explaining 95% of the shape variation. Life cycle has a highly significant influence on the shape of all cranial regions (Supplementary Table 2), with species that share the same life cycle clustering together in cranial morphospace (see Fig. 2 and Extended Data Fig. 4 for the results on fine-grained classifications). In contrast, microhabitat (see Methods) is a significant influence on only four individual elements and on overall cranial shape, at much lower significance levels (Supplementary Table 3), and does not clearly discriminate species in the cranial morphospace beyond its interaction with life cycle (Supplementary Fig. 5). PC1 (>31% of the overall shape variation) segregated species with a fully aquatic life cycle (paedomorphic) from species with either a fully (viviparous, direct-developing) or largely (biphasic) terrestrial life cycle. Variation along this axis also corresponds to the degree of metamorphosis, from differential to complete metamorphosis. Aquatic paedomorphic species are elongated with a reduced number of bones, whereas more terrestrial species have a complete and more robust skull (Fig. 2). PC2 (>19% of the overall shape variation) described differences between species with aquatic and terrestrial life cycles, with fully terrestrial, direct-developing plethodontids clearly differentiated from other species that spend some or all of their lives in water, including a number of troglodytic plethodontids. These differences between fully aquatic species and fully or primarily terrestrial species are even more evident in the phylogenetic principal component analysis (PCA) (Extended Data Fig. 5). Shape differences along PC2 are mainly concentrated on the pterygoid and vomer, with terrestrial, direct-developing species showing a more gracile cranium without a pterygoid and with a vomer lacking the transverse series of teeth. Paedomorphic species occupy the largest area of the morphospace, followed by biphasic species. Notably, the direct-developing plethodontids (the most species-rich clade of salamanders) occupy only a small area of the morphospace described by the first two PC axes.

**Cranial diversity is influenced by life cycle.** We tested for differences in morphological diversity depending on life cycle (Extended Data Fig. 6 and Supplementary Data 1) to explore the overall morphological pattern. Aquatic paedomorphic species show a higher disparity of cranial shape than species with other types of life cycle (as well as relative to other more fine-grained categories, Extended Data Fig. 6) and associated habitats. Direct-developers exhibit low disparity, whereas biphasic species are intermediate between direct-developers and paedomorphic taxa (Extended Data Fig. 6).

## Transitions in the life cycle influence the rate of cranial evolution.

We performed an ancestral reconstruction of the different life-history strategies (Fig. 3, Extended Data Fig. 7 and Supplementary Tables 4 and 5) and estimated the rates of cranial evolution across the Caudata phylogeny (Fig. 4). Our results support a biphasic life cycle as the ancestral condition for Caudata (Fig. 3 and Extended Data Fig. 7), with paedomorphosis evolving independently in several lineages. Furthermore, the biphasic life cycle re-evolved several times in lungless salamanders (plethodontids, Fig. 3). Fast evolution of cranial shape occurred in lineages leading to paedomorphic species and biphasic species (Fig. 4 and Extended Data Figs. 8 and 9). Direct-developers have a relatively lower rate of cranial evolution. Major shifts in the rates of cranial evolution occurred early in the evolution of salamanders and were followed by transitions in life cycle strategies. For example, during the Mesozoic, major shifts in the cranial evolution rate occurred at the transition between the paedomorphic Sirenoidea and the species-rich Salamandroidea, as well as within the families of the latter clade, which vary considerably in life history. Another major shift in the rate of cranial evolution occurred between the paedomorphic Cryptobranchidae and the biphasic Hynobiidae. The relationship between rates of morphological evolution and life history transitions is particularly evident within two genera, the plethodontid *Eurycea* and the ambystomatid *Ambystoma*

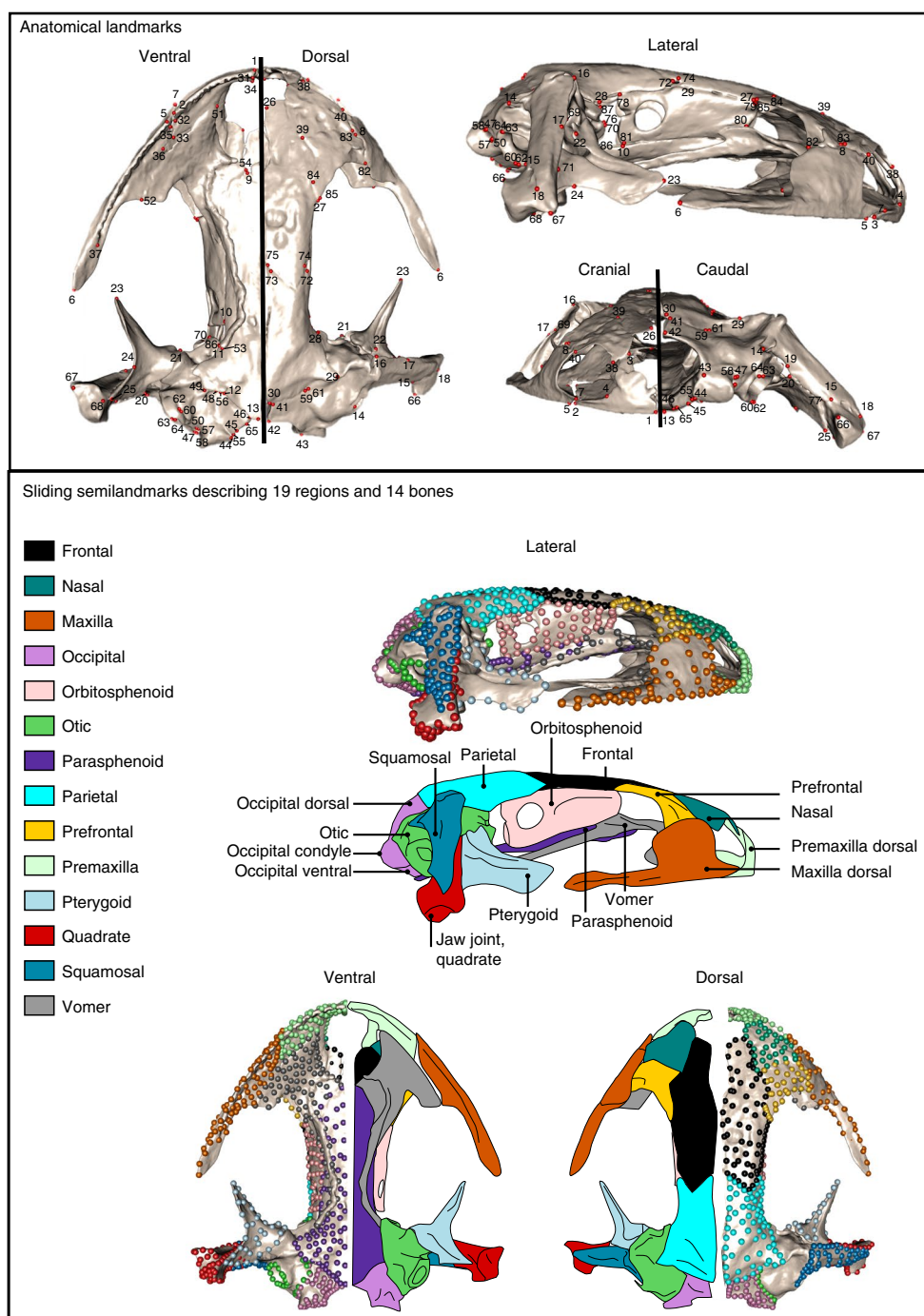


**Fig. 1 | Landmarks used to quantify cranial shape variation in Caudata.** The top panel shows anatomical landmarks placed on a scan of *Salamandra salamandra* and corresponding to the definitions in Supplementary Data 9. The red dots represent the anatomical landmarks. The bottom panel shows sliding semilandmarks that describe the 14 bones of the cranium used in all shape analyses. A representative species for each family is also provided in Extended Data Figs. 1–3.

(Figs. 3 and 4), which both include metamorphosing and paedomorphic species. In both genera, the shift to a paedomorphic life cycle, which is accompanied by a reversal to an aquatic environment, is associated with an increase in the rate of cranial evolution.

**Species with complete metamorphosis are more modular than paedomorphic species.** We found that species exhibiting complete metamorphosis (biphasic with 12 modules and a covariance ratio (CR) of 0.61; direct-developing species with 13 modules

and  $CR = 0.54$ ; Fig. 5a,b,d,e) exhibit more modular skull evolution than paedomorphic species (11 modules and  $CR = 0.71$ ; Fig. 5c,f and Supplementary Data 2–4). These results hold after subsampling our samples of biphasic and direct-developing species to match the sample size of paedomorphic species (after subsampling,  $CR_{bi} = 0.63$ ;  $CR_{dd} = 0.56$ ; Supplementary Data 5 and 6). Our analyses further demonstrate that the suspensorium (composed of the squamosal, quadrate and pterygoid) and the maxilla have high within-region evolutionary integration across caudates.

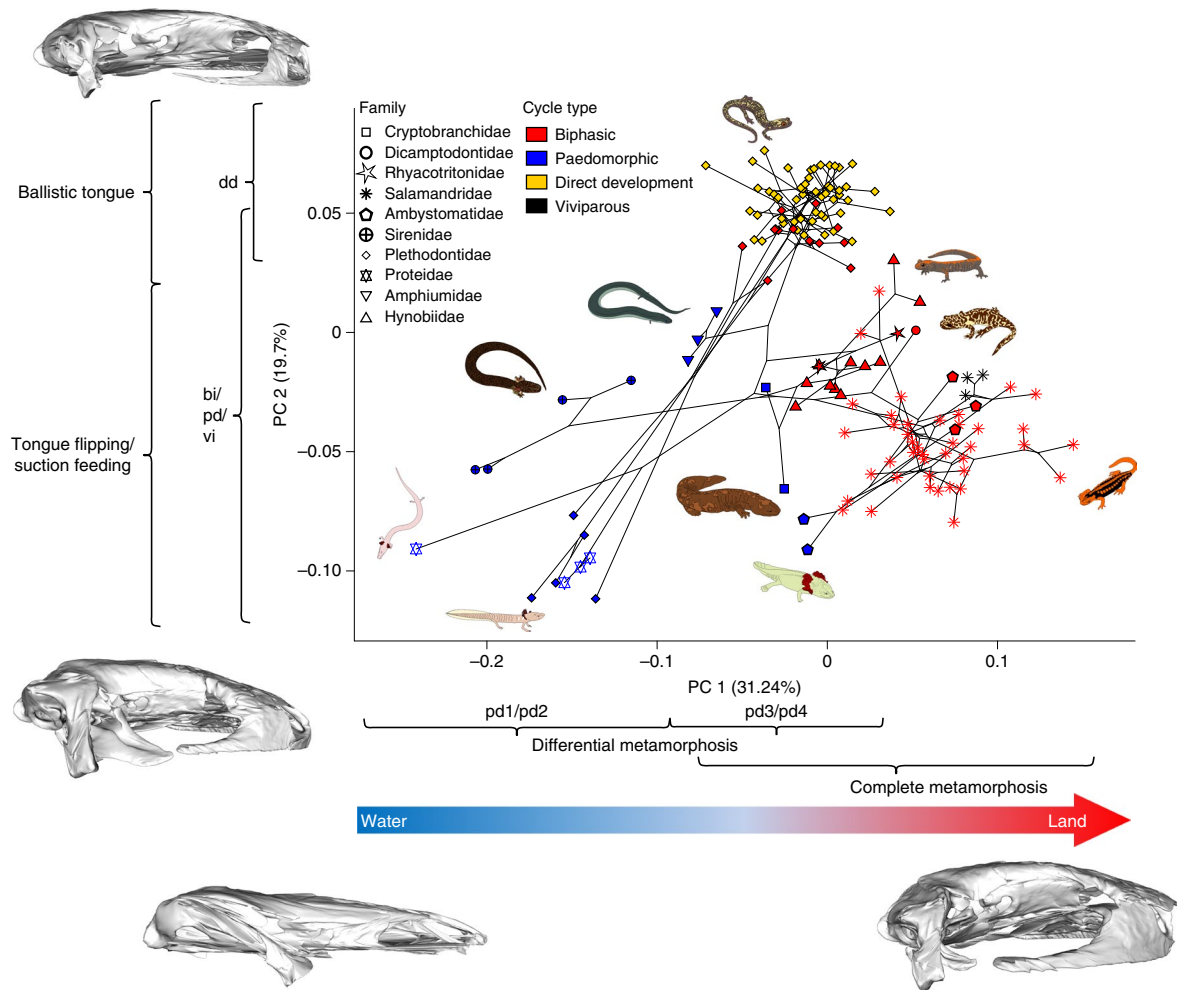


**Fig. 2 | Phylomorphospace illustrating the first two PCs of cranial shape across Caudata.** The symbols indicate family-level clades, and the colours represent life cycle strategies. Skull shapes at the positive and negative extremes of each axis are depicted with warped surfaces. The abbreviations are as follows: bi indicates biphasic species, or species that are considered biphasic; dd indicates direct-developing species; pd indicates strictly paedomorphic species; pd1 indicates paedomorphic species with external gills, gill slits, a tail fin, no eyelids, no maxillary bones, no septomaxilla and no prefrontal; pd2 indicates paedomorphic species with external gills, gill slits, a tail fin, no eyelids, no septomaxilla, no prefrontal and with maxillary bones developing before adulthood; pd3 indicates paedomorphic species without external gills but with gill slits, a tail fin, no eyelids, no septomaxilla and with maxillary and prefrontal bones developing before adulthood; pd4 indicates paedomorphic species with external gills, gill slits, a tail fin, no eyelids, no septomaxilla and with maxillary and prefrontal bones developing before adulthood; vi indicates strictly puereparate viviparous species. See Extended Data Fig. 4 for the results on finer-grained classifications.

**Per-module rate and disparity are correlated only in completely metamorphic species.** We tested the tendency to evolve disparate morphologies depending on life cycle by assessing the relationship between the rate of evolution and the disparity for each module. Results of the Spearman correlation ( $\rho_s$ ) show a positive relationship between the rate of cranial evolution and the disparity in both biphasic ( $\rho_s = 0.72$ ;  $P = 0.01$ ; Fig. 5g) and direct-developing species ( $\rho_s = 0.7$ ;  $P = 0.009$ ; Fig. 5h), with the suspensorium and the maxilla evolving at the highest rates of any cranial region. No correlation was found in paedomorphic forms (Fig. 5i).

**Per-landmark relationship between rate and disparity differs between completely metamorphic and paedomorphic species.** Comparing the relationship between disparity and evolutionary rate with the relationship expected under a constant rate of Brownian motion evolution can reveal instances of facilitation (disparity is higher than expected) or constraint (disparity is lower than expected). In biphasic species, disparity is lower than expected for nearly all cranial bones except for the vomer and the pterygoid which

show instead a relatively higher disparity (Fig. 6). Direct-developing species show a similar pattern to biphasic species, with higher disparity than expected given the estimated rate of evolution for the vomer; while nearly all the other elements (maxilla, nasal and parietal) fall within the expectation of a Brownian motion process (Fig. 6). In contrast, in paedomorphic species, some cranial elements such as the parietal, frontal, vomer, orbitosphenoid, occipital and parasphenoid display lower disparity than expected given the estimated rate of evolution. Only the maxilla and nasal show a high disparity relative to the estimated rate, and all other cranial bones in paedomorphic species follow the expectation of a Brownian motion model of evolution (Fig. 6).

## Discussion

Metamorphosis requires substantial ecological, functional and morphological transformations through ontogeny, and yet is ubiquitous across animals<sup>8,37</sup>, including half of all living vertebrates<sup>8</sup>. However, its impact on morphological diversity remains poorly understood. Our results indicate that species with different life cycles

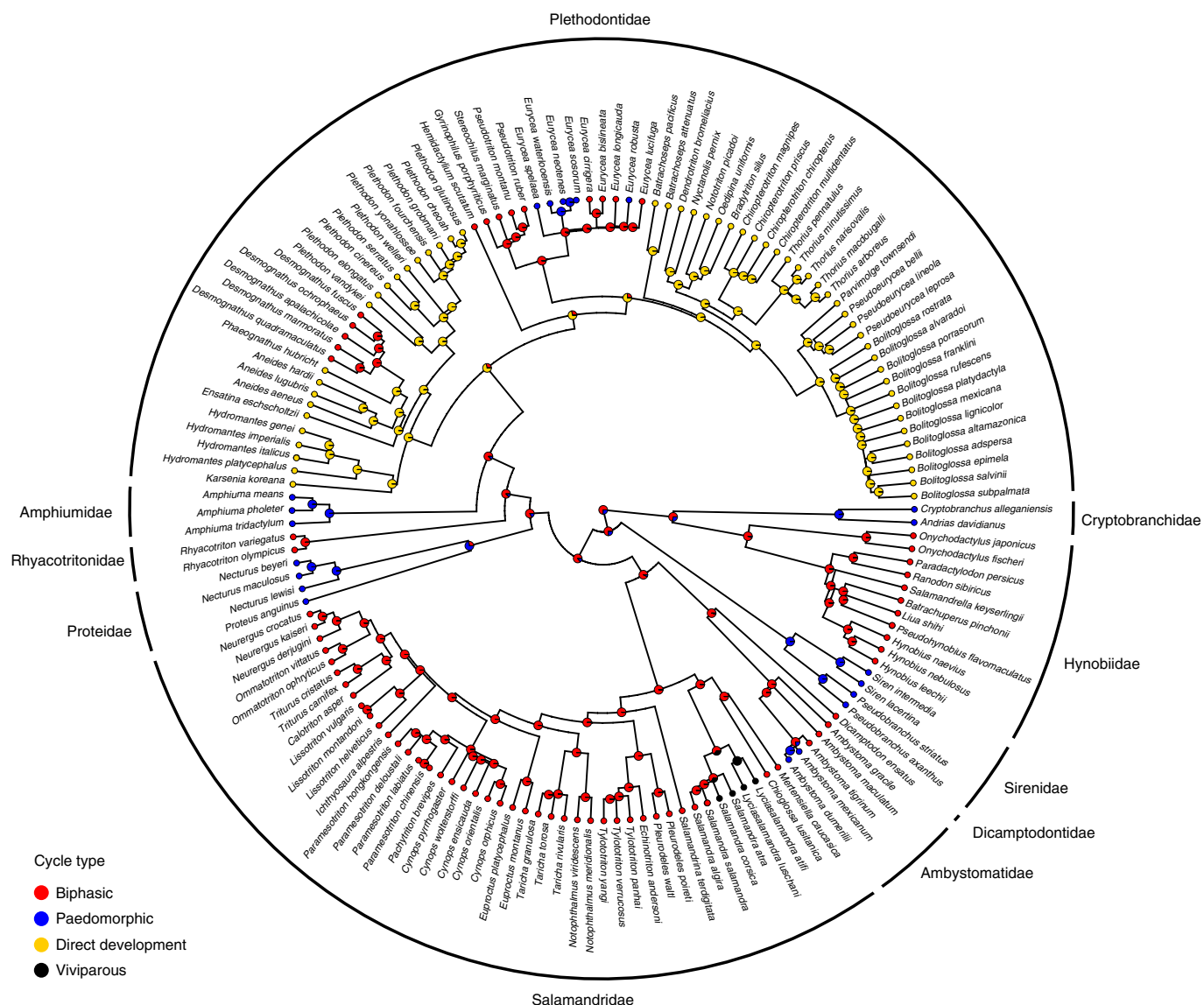


**Fig. 3 | Evolution of the life cycle in Caudata.** Ancestral state estimation using a rerooting method performed on the symmetric rate model (the best model following the results of the Akaike information criterion (AIC), Supplementary Table 4). The colours indicate life cycle strategies. See Extended Data Fig. 7 for the results on finer-grained classifications.

have distinct evolutionary patterns for adult cranial morphology. Changes in cranial shape along the main axis of variation followed a gradient of metamorphosis associated with habitat use as well as feeding mode. The cranial shape of paedomorphic species with differential metamorphosis is streamlined, with a reduced number of bones, probably related to both aquatic and suction-feeding adaptations<sup>38–40</sup>. In addition, aquatic species with more complete differential metamorphosis (cryptobranchids and some ambystomatids) tend to have wider heads, probably related to suction feeding, as wider heads allow for greater volume expansion during jaw opening. In contrast, species exhibiting complete metamorphosis (biphasic and direct-developing species, including most salamanders, plethodontids, rhyacotritonids, hynobiids and ambystomatids) have a more complete and robust cranium, as well as a more terrestrial habitat and a tongue-based feeding strategy. Among these terrestrial feeders, most biphasic species using tongue protrusion coupled with jaw prehension display a more robust suspensorium (composed of the pterygoid, quadrate and squamosal) than many

of the direct-developing species with a long-tongued ballistic feeding mode. Paedomorphic species occupy a large area of the morphospace and exhibit the highest disparity, suggesting multiple routes to their simplified and larval-like morphology. These species include taxa that undergo differential metamorphosis (for example, Amphiumidae, Cryptobranchidae and Ambystomatidae) that are similar in shape to fully biphasic species, as well as species that retain nearly all larval traits into adulthood (for example, Proteidae, Sirenidae and some *Eurycea*). Notably, the direct-developing plethodontids, the most species-rich clade of salamanders, occupy the smallest area of the morphospace and have the lowest disparity.

Developmental canalization is hypothesized to reduce morphological variation in species with multistage life cycles (biphasic)<sup>25</sup>. Our results show that species exhibiting complete metamorphosis (including both biphasic and direct-developing forms) are less disparate than those that undergo differential metamorphosis (that is, paedomorphic forms). Thus, it is the process of complete metamorphosis (whether occurring at the larval stage or *in ovum*), and

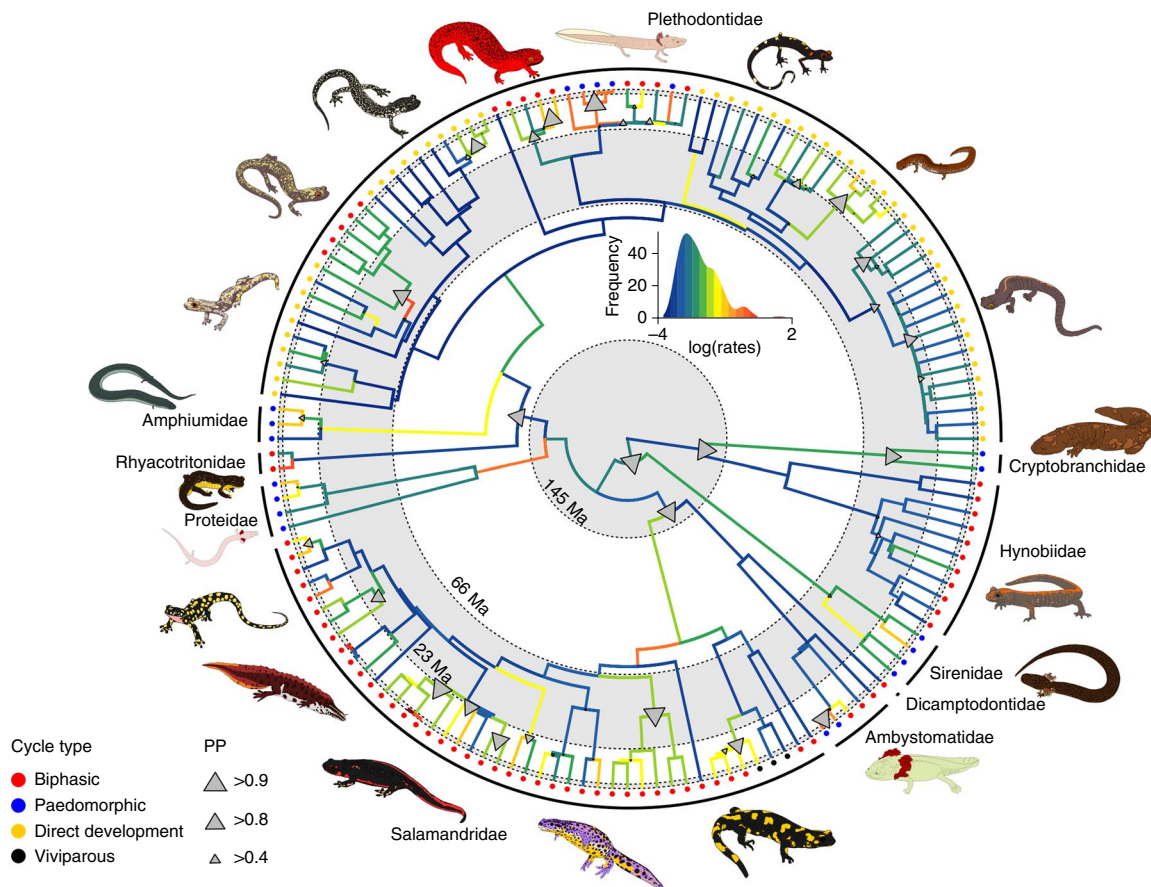


**Fig. 4 | Evolutionary rates and rate shifts for cranial shape in Caudata.** The colour gradients on the branches indicate the rates of shape evolution, with warmer colours corresponding to higher rates and cooler colours to lower ones. Frequencies of the log-transformed rates of cranial shape evolution are indicated by the distribution plot. The grey triangles indicate the stem branches of clades with support for whole-clade shifts in evolutionary rate. The posterior probabilities (PP) of the rate shifts are indicated by the relative sizes of the triangles (Extended Data Fig. 10). The rates and shifts were estimated using BayesTraitsV3 using a variable-rates Brownian motion model. Times in the tree are indicated in millions of years (Ma). See Extended Data Fig. 9 for the results on finer-grained classifications.

not merely the presence of a multistage life cycle, that may canalize cranial shape variation in salamanders.

Changes in developmental strategy have impacted the dynamics of body form and limb evolution in salamanders over the past ~160 million years<sup>25,33</sup>. As shown in previous studies, a biphasic life cycle was recovered as the ancestral condition for Caudata<sup>41,42</sup>, with direct-development evolving once, paedomorphy evolving several times independently<sup>25,29,31</sup> and biphasic (and sometimes then paedomorphic) strategies evolving and re-evolving multiple times among direct-developing plethodontids. Changes in developmental strategy are consistently associated with shifts in the rate of cranial evolution, with paedomorphic and biphasic species showing faster rates than terrestrial direct-developing species. Furthermore, a reversal from a terrestrial biphasic to an aquatic paedomorphic life cycle is also accompanied by an increase in the rate of cranial evolution, as found in Ledbetter and Bonett<sup>33</sup>. These results suggest that the rapid morphological evolution in paedomorphic taxa, which tend to live in inhospitable environments with poor access to food resources and mates (such as caves or organic muck habitats)<sup>31,43</sup>, may facilitate the persistence of these species in such challenging conditions<sup>44,45</sup>. In contrast, complete terrestriality in direct-developing plethodontids may impose strong constraints on their cranial shape evolution, possibly associated with ballistic tongue projection. This constraint is demonstrated by a low disparity and rate of evolution in this group, as previously also documented for limb morphology<sup>33</sup>. However, in contrast to previous studies, we did not

find that direct-developing species (even if they remain in the same environment during their entire life) have a higher rate of evolution than biphasic forms<sup>25</sup>, suggesting that cranial shape and body form are differentially impacted by developmental strategies. Moreover, our results on cranial shape do not support those obtained at the intraspecific level in *Triturus* newts, where metamorphosis did not induce reduced variability in external head shape<sup>26</sup>, which may suggest distinct processes at the micro- and macroevolutionary scales.

Our analysis of patterns of evolutionary integration and modularity in species with different life cycles recovered a more modular pattern than documented in previous studies of the caudate skull<sup>46,47</sup>. As expected, paedomorphic species have a more integrated cranium than biphasic and direct-developing ones (the latter of which undergo prehatching metamorphosis)<sup>48</sup>. The fact that direct-developing species have a (slightly) more modular cranium than biphasic forms is surprising and suggests that the impact of metamorphosis on cranial organization and evolution is retained even when the larval stage is entirely *in ovum*. Analyses of phenotypic integration and modularity within *Salamandra salamandra*<sup>49</sup> support the same pattern as observed at the evolutionary level, suggesting that the recruitment of all the bones of the suspensorium (pterygoid, jaw joint, quadrate and squamosal) into one strongly integrated, quasi-autonomous module may have facilitated its evolvability, resulting in a high rate of evolution and disparity for the bones of the suspensorium across Caudata. This pattern may relate to changes in feeding mode during metamorphosis, which

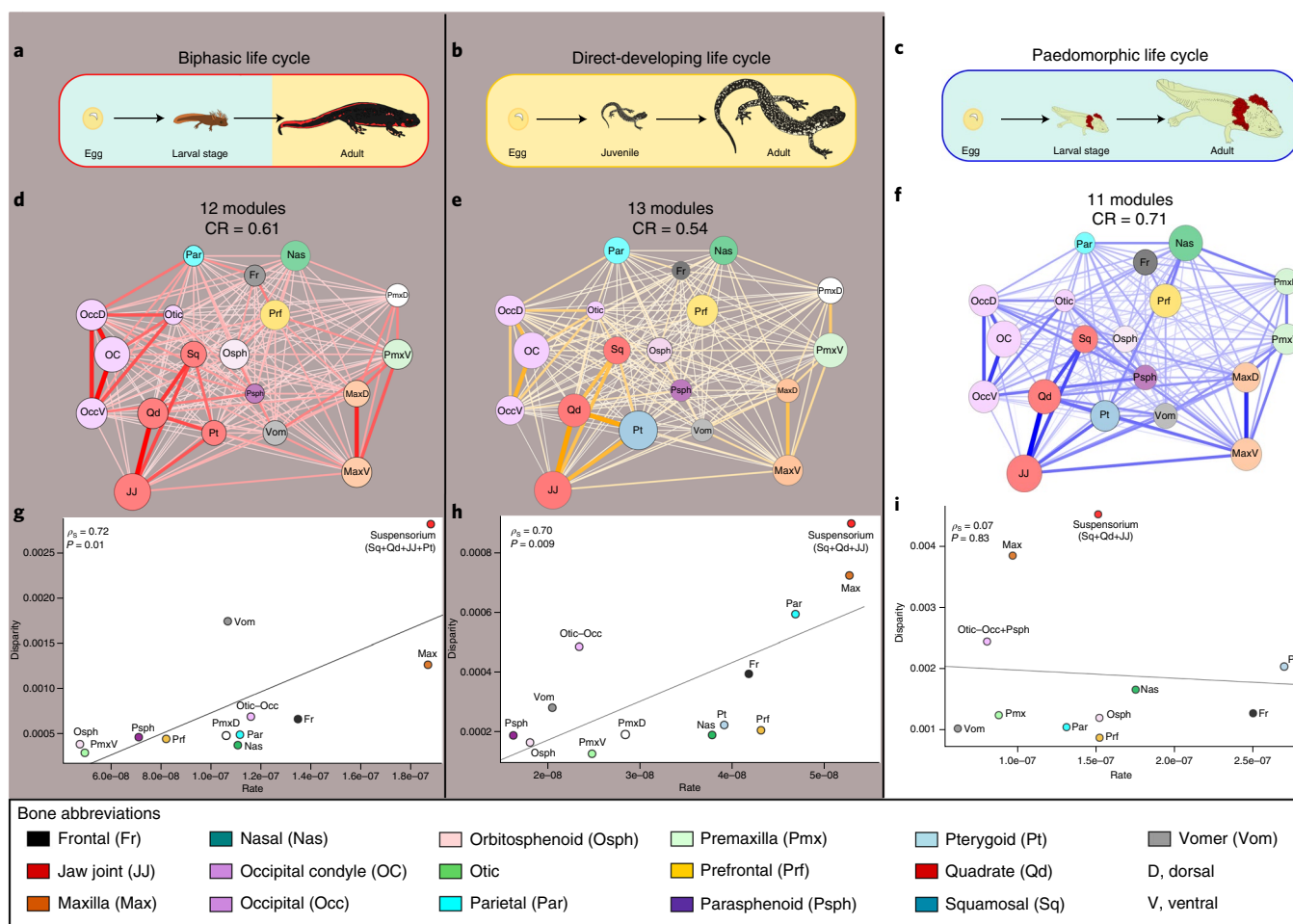


**Fig. 5 | Modularity and integration in cranial shape for different caudatan life cycle strategies.** **a–c**, Schematics of each life cycle strategy are provided in biphasic (**a**), direct-developing (**b**) and paedomorphic (**c**) life cycles. Changes in the environment are represented by colours, with light blue for an aquatic environment and yellow for a terrestrial environment. The grey background indicates life cycles involving full metamorphosis, with (**a**) or without (**b**) a free-living, actively feeding larval stage. **d–f**, Network graphs indicating integration within and between regions and the respective CRs for the indicated models. The networks illustrate the groupings of the 19 cranial regions using phylogeny-informed EMMI analysis. The regions were grouped as modules (and coloured accordingly) when the between-region correlation (the thickness of the line in the network graph) was within 0.2 of the lowest internal correlation (indicated by circle size in the network graph). **g–i**, Procrustes variance versus the rate per module and the linear regression of the observed rate–variance relationship.

requires a radical change in morphology and ecology<sup>24,50,51</sup> and induces skull remodelling involving primarily the feeding apparatus. Unexpectedly, direct-developing species exhibit similar patterns to biphasic species, despite undergoing metamorphosis without an actively feeding larval stage. Our results thus suggest that metamorphosis in any form strongly impacts the pattern of shape evolution of the cranial bones.

We further tested the hypothesis that metamorphosis strongly impacts the pattern of cranial shape evolution by assessing the per-landmark Procrustes variance and mean evolutionary rates for each cranial element in biphasic, direct-developing and paedomorphic species. Our results show that, in biphasic species, nearly all the cranial bones are constrained (with a low disparity relative to their respective rates of evolution) except for those that are remodelled during metamorphosis (with a high disparity relative to rate for the vomer<sup>52</sup> and the pterygoid). The pattern is similar in direct-developing species except that nearly all cranial bones follow a Brownian motion model of evolution, where the disparity of each is increasing in line with its respective evolutionary rate. However, the overall pattern is different in paedomorphic species, where most of the bones show a high heterogeneity of disparity relative to rate,

even within bones (see the orbitosphenoid in Fig. 6). This difference may reflect variation due to differential levels of metamorphosis in paedomorphic taxa<sup>29,50</sup>, as is evidenced by the variable absence of some bones (maxilla, prefrontal, nasal and orbitosphenoid).

### Conclusions

Metamorphosis is one of the most fascinating, spectacular and surprisingly common developmental processes in the animal kingdom<sup>8,23</sup>, often requiring an abrupt change in morphology and ecology during the lifetime of an individual as it transforms from a larva into an adult. Despite the potential for metamorphosis to impose compounding constraints on morphological evolution, our analyses suggest that completely metamorphic species, with or without an actively feeding, free-living larval stage, exhibit a high evolutionary autonomy of the cranial elements. This autonomy probably promotes the diversification of metamorphic (or ancestrally metamorphic) species by allowing the rapid evolution of structures that engage in divergent functions and thus experience dynamic selection pressures both during ontogeny and through evolutionary shifts in life cycle complexity. The origin and evolution of different life-history stages, their maintenance through time and their impacts on species

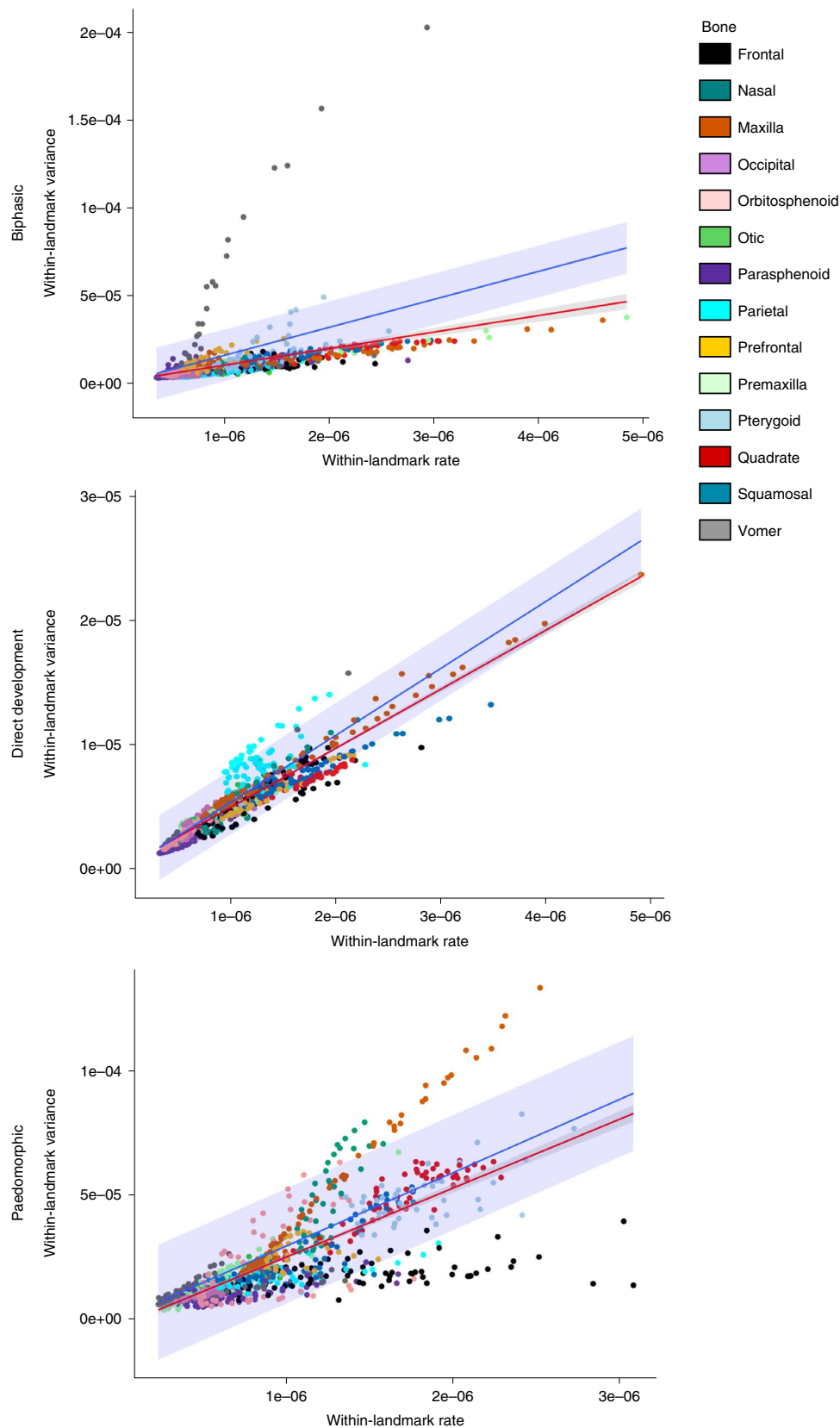


**Fig. 6 | Per-landmark evolutionary rate against Procrustes variance for different caudatan life cycle strategies.** Results for biphasic (top), direct-developing (centre) and paedomorphic species (bottom). The red lines and grey areas represent the linear regressions of the observed within-landmark rates and variances and their 95% confidence intervals, respectively. The blue lines and blue areas indicate the expected relationships between within-landmark rates and variances given a Brownian motion model of trait evolution and their 95% confidence intervals, respectively.

diversification still remain poorly understood and merit further attention. Future research using longitudinal series with specimens at different developmental stages at the micro- and macroevolutionary levels is necessary to better understand how and why metamorphosis is an important driver of cranial diversity.

## Methods

**Data sampling.** We sampled 152 specimens belonging to 148 species and representing all families of Caudata (Supplementary Data 7) for this study. This sample was selected to represent the diversity of developmental life cycles within each family as fully as possible.

**Developmental life cycle traits and microhabitats.** Developmental life cycle and microhabitat data were collected for each species from the existing literature (Supplementary Figs. 1–3 and Supplementary Data 8). The following definitions are used for each life cycle. Species are defined as paedomorphic (pd) when they retain aquatic larval traits when reproductively active. Species are defined as direct-developers (dd) when they fully transform in the egg and hatch directly as terrestrial miniature versions of the adults. Species are defined as biphasic (bi) when they exhibit a multiphasic life cycle (most of them exhibit a two-part life cycle), with an aquatic larval stage followed by metamorphosis into a more terrestrial adult<sup>25,41,53</sup>. Because direct-developers undergo metamorphosis in the *ovum*, we consider both biphasic and direct-developing species as metamorphic. It is important to note that this classification is an oversimplification of life cycle categories in some species. Some species in our dataset are facultative biphasic, where some populations can be either metamorphs or paedomorphs, and this is often associated with changing habitats (Supplementary Data 8). Other species are defined as puereparate viviparous when they have embryos developing inside their bodies until the end of gestation, and they give birth to fully developed terrestrial juveniles (or stricto sensu pueriparity in this study)<sup>54</sup>. Some species are facultatively viviparous, and these are mainly larviparous in our dataset (Supplementary Data 8), delivering small aquatic larva in the water. Because neither of the two facultative viviparous species (*Salamandra atra* and *Salamandra atra*) in our dataset are puereparate<sup>54</sup>, we treat them as biphasic species in further statistical analyses (phylogenetic multivariate analyses of variance (MANOVAs), and modularity and integration analyses), as they still have an active larva and encounter a full metamorphosis with a change of morphology and ecology. The strictly puereparate viviparous species were not included in several statistical analyses (such as the phylogenetic MANOVAs and modularity and integration analyses), as they are represented by only three species in our dataset (*Lyciasalamandra atifi*, *Lyciasalamandra luschani* and *Salamandra atra*). Another important point to raise is the complexity of the paedomorphic category, which includes several species that encounter differential metamorphosis<sup>29,50</sup>, with variation of the composition of larval traits retained into adulthood. Using the literature<sup>29,50</sup>, we defined four different categories of paedomorphy depending on the traits that are modified during metamorphosis (Supplementary Data 8). Variability is also present among biphasic species with facultative biphasic species, where some populations can be paedomorphic. Other species that are coded as biphasic in all our analyses are in fact multiphasic, such as *Notophtalmus*<sup>55</sup> (which have an aquatic larva, a terrestrial juvenile and an aquatic adult) or *Ichthyosaura alpestris* and *Lissotriton vulgaris* (which seasonally change between an aquatic and a terrestrial life as adults)<sup>56</sup>.

While the coding of life cycles is necessarily oversimplified here for the purposes of robust statistical analyses, we encourage readers to consider the appropriateness of this coding scheme and possibilities of capturing more nuanced categories in future work. Nevertheless, at present, finer levels of classification cannot be used in most of our analyses, as we need more than 20 species (ideally 30 species) per group for the modularity and integration analyses, and at least 5 species per group to test for shape differences depending on the life cycle, disparity and rate of evolution. Microhabitats (semi-fossorial, aquatic, semi-aquatic, terrestrial, arboreal, aquatic species living in caves and terrestrial species living in caves) were defined as a finer scale than the broad habitats associated with life cycle (terrestrial and aquatic).

**Three-dimensional scanning and processing.** We generated 107 scans for this study (107 species) and collected 45 from different online repositories (Supplementary Data 7). The following CT scanners were used to scan specimens at high resolutions: a Phoenix VTX L240-180 CT scanner (General Electric) at the X-ray tomography facility at the Museum National d'Histoire Naturelle (AST-RX platform, UMS 2700); a Phoenix nanotom X-ray[s] at the Museum für Naturkunde; a Phoenix VTomex M240 at the University of Florida's Nanoscale Research Facility and made available on MorphoSource ([morphosource.org](http://morphosource.org)); and a Nikon Metrology HMX ST 225 CT scanner at the CT facility of the Natural History Museum. The specimens collected from Digimorph ([digimorph.org](http://digimorph.org)) were scanned using an ACTIS scanner at the High-Resolution X-ray Computed Tomography Facility at the University of Texas at Austin. Avizo Lite 9 (FEI Visualization Sciences Group) was used to segment and export the skull reconstructions of each specimen as PLY files. All the PLY files were imported into Geomagic Wrap (3D Systems) to clean, repair and decimate the meshes before the landmarking procedure.

**Quantification of skull shape using three-dimensional geometric morphometrics.** The extreme variability in cranial region presence and morphology between metamorphic and non-metamorphic species has so far hindered robust comparisons of cranial shape using traditional morphometric approaches (Fig. 1 and Supplementary Data 9). To comprehensively capture cranial morphology across Caudata, we used a high-density surface geometric morphometric approach. We used 87 landmarks, 496 curve sliding semilandmarks and 356 surface sliding semilandmarks to delineate 14 cranial regions (Fig. 1 and Supplementary Data 9). A three-dimensional sliding-semilandmark procedure<sup>57–59</sup> was used to precisely quantify the shape of each skull bone. This method allows the comparison of different shapes by transforming sliding semilandmarks on curves and surfaces into spatially homologous landmarks<sup>60</sup>. All the landmarks and curve semilandmarks were manually collected by the same person (A.-C.F.; Fig. 1 and Supplementary Data 9) using the software package IDAV Landmark v.3.0.0.6<sup>61</sup> (<http://graphics.idav.ucdavis.edu/research/EvoMorph>) and following the protocols described in several previous studies<sup>62–67</sup>. The curve semilandmarks generated from IDAV Landmark were subsampled using the algorithm of Botton-Divet et al.<sup>68</sup>. Next, all the surface sliding semilandmarks were obtained using a semi-automated approach in the Morpho R package v.2.5.1<sup>69</sup>. We first created a template with the same configuration of landmarks and curve semilandmarks plus surface semilandmarks. To do so, we created a hemispheric template mesh using a 360 × 360 uniform-vertex sphere created in Meshlab (<http://www.meshlab.net/>) and modified in Blender (Stitching Blender Foundation), on which we manually placed all the landmarks and the curve and surface sliding semilandmarks. We then used this template to place surface semilandmarks semi-automatically onto each specimen by fitting the template's coordinates (landmarks and curve semilandmarks) to those of each specimen. Surface semilandmarks were placed using the placePatch function<sup>69</sup>, which determined their position through a thin-plate spline method. Each bone was patched separately following protocols as described elsewhere<sup>59,65</sup>. For a more accurate patching, different 'inflate' values across partitions and specimens were used because of the wide range of size and shape differences in our sample. Finally, all the sliding semilandmarks were slid to minimize bending energy criteria using the functions RelaxLM and slider3d<sup>69</sup>.

All salamander species have nine cranial regions corresponding to ten bones that are invariably present (the otic region (including both prootic and opisthotic bones), occipital, premaxilla, frontal, parietal, parasphenoid, squamosal, quadrate and vomer), but some cranial bones are variably present across the order (pterygoid, maxilla, prefrontal, orbitosphenoid and nasal; Extended Data Figs. 1–3 and Supplementary Data 10). To represent the whole shape of the skull and to be able to compare cranial shape across the entire dataset, we decided to represent these absent regions by one landmark position (the position was chosen as best representing the location of the missing region). This was achieved by replicating this one landmark and forming an array with the same dimensions as the surface point dataset from specimens with that bone present<sup>66,70</sup>. Thus, an absent region is represented in this dataset as an infinitesimal surface, corresponding to exactly the same dimensions as those of a present region. This approach allows us to include all specimens and bones in the analyses. Because data were recorded on only the right side of each specimen, and to avoid alignment artefacts during the Procrustes superimposition<sup>71</sup>, the landmarks and semilandmarks were mirrored using the mirrorfill function in the paleomorph R package v.0.1.4. Finally, a global Procrustes alignment was performed using the gpgan function in the geomorph R package v.3.1.2, and the missing regions had a non-zero (but negligible) size<sup>66</sup>. A mean shape was calculated for each species using the Procrustes coordinates and was used in all further analyses.

**Phylogenetic tree.** Comparative analyses were performed on the maximum clade credibility (MCC) tree estimated from a posterior sample of 1,000 trees published by Jetz and Pyron<sup>72</sup>. The MCC was calculated using the TreeAnnotator program in BEAST<sup>73</sup> using the CAT (common ancestor tree) algorithm to avoid issues with the estimation of negative branch lengths<sup>74</sup>. This MCC tree was pruned to the species present in our dataset for further comparative analyses. Because some species were not present in the phylogeny, we substituted them with species that are closely related. Thus, *Thorius tlaxiacus*, *Thorius pinicola* and *Tylostotriton himalayanus* from our dataset were substituted in the phylogeny by *Thorius arboreus*, *Thorius macedougalli* and *Tylostotriton yangi*, respectively, following previous studies<sup>75,76</sup>. Finally, we scaled the MCC tree using the branch-specific average rates obtained from the posterior samples of the Bayesian analyses (see 'Estimation of branch-specific evolutionary rates and rate shifts'). This tree was used in the downstream phylogenetic comparative analyses (phylogenetic MANOVAs, phylogenetic modularity and correlation between disparity and rate per landmark) and has the advantage of taking into account the heterogeneity in rates that have been estimated by the Bayesian approach.

**Data analyses. Cranial morphological variation. Impact of size on cranial shape.** To assess the impact of size on shape, we used the centroid size as proxy of cranial size for each species. We performed a phylogenetic regression using the function procD.pgls from the geomorph R package v.3.1.2<sup>77,78</sup> using the Procrustes coordinates, the log<sub>10</sub> of the centroid size and the scaled MCC tree. Phylogenetic regressions were performed on four different Procrustes superimposed datasets:

(1) the full dataset containing all the species, (2) the biphasic dataset, (3) the direct-developing dataset and (4) the paedomorphic dataset. Depending on the impact of the size on shape, further analyses were performed on the Procrustes coordinates after accounting for centroid size and phylogeny.

**Visualization and test for shape differences.** Shape differences were visualized using a PCA as well as a phylogenetic PCA on which the phylogeny was mapped using the function `phylo.morphospace` from the `phytools` R package v.0.6-99<sup>79</sup>. To assess whether cranial shape differs depending on life cycle, we performed phylogenetic MANOVA using the function `procD.pgl` from the `geomorph` R package v.3.1.2<sup>77</sup>.

**Disparity differences.** To assess and compare morphological disparities for each life cycle strategy (biphasic, paedomorphic and direct-development) we used the function `morphol.disparity` in `geomorph` v.3.1.2. Disparity is calculated as the Procrustes variance divided by the number of landmarks per bone for each life cycle using the residuals of a linear model fit<sup>80</sup>. Pairwise comparisons to identify differences among groups were also performed.

**Evolutionary rates.** Calculations of evolutionary rates for the whole cranial shape as well as for each cranial element and comparisons across different life cycle strategies were performed on the basis of a Brownian motion model of evolution using the function `compare.multi.evol.rates` in the `geomorph` R package v.3.1.2.

**Transitions of life cycle and rates of cranial evolution. Estimation of branch-specific evolutionary rates and rate shifts.** The rates of evolution in the salamander skull were analysed using the variable rates model implemented in `BayesTraitsV3` (<http://www.evolution.rdg.ac.uk/>). A reversible-jump Markov chain Monte Carlo algorithm was used to detect shifts in the rates of continuous trait evolution (modelled by a Brownian motion process<sup>81</sup>). We used as input traits the phylogenetic PCs accounting for 95% of the overall variation in shape for the whole cranium (the first 42 phylogenetic PCs). Four independent chains were run for 200,000,000 iterations, sampling every 10,000 iterations, and the first 25,000,000 iterations were discarded as burn-in. Trace plots were examined to ensure that the chains were stationary after burn-in. The effective sample size (ESS) of the posterior samples (ESS > 100) was assessed using the `effectiveSize` function, and the convergence of the chains was assessed using Gelman and Rubin's convergence diagnostic<sup>82</sup> (function `gelman.diag`); both functions are implemented in the R package `coda` v.0.19-3 (Supplementary Fig. 6 and Supplementary Tables 6 and 7). The results of the analyses were plotted on the tree using the function `mytreebybranch` (<https://github.com/anjoswami/salamanders/blob/master/mytreebybranch>) and summarized by the branch-specific average rate and the posterior probability of rate shifts, both estimated from the posterior samples using the `rjpp` and `plotShift` functions in the `btrtools` R package v.0.0.0.9000 (<https://github.com/hferg/btrtools/tree/master/R>).

**Ancestral state estimation of the life cycle in Caudata.** Ancestral state estimations were conducted to compare the positions of shifts in the rates of morphological evolution with the acquisitions of the different life cycles in Caudata. We used a Markov model<sup>83</sup> for estimating the past transitions between life cycles at internal nodes in the phylogeny. The model fit was performed assuming that the transition rates between character states are either all equal, different for each state but symmetric, or asymmetric, using the algorithm implemented in the `rerootingMethod` function in `phytools` v.0.6-99<sup>79</sup>. The best model was selected using the AIC<sup>84</sup> (Supplementary Tables 4 and 5).

**Cranial modularity and integration.** To test whether the developmental strategy (complete metamorphosis in biphasic and direct-developing species versus differential metamorphosis in paedomorphic species) and whether the change in ecology during development (change of diet and environment in biphasic species versus no change of diet and environment in direct-developing and paedomorphic species) impact the evolutionary integration in salamanders, we assessed the pattern and magnitude of phenotypic modularity and integration for each dataset depending on developmental strategies (biphasic, direct-developing and paedomorphic). Cranial modularity was estimated using two methods developed for testing the degree of morphological integration with high-dimensional data. The first method is a maximum-likelihood approach, which calculates AIC<sup>84</sup> values to assess the best-supported model of modularity on the basis of trait correlations. This is conducted using the function `EMMLi` from the `EMMLi` R package v.0.0.3<sup>85</sup>. The second method used is CR analysis, which assesses the covariances within and among hypothesized modules and compares this ratio with a null hypothesis of random assignment of shape variables to partitions<sup>86</sup>. Covariance ratios were estimated using the `modularity.test` function from the `geomorph` R package v.3.1.2<sup>77</sup>. Different hypotheses of evolutionary modularity were tested (Supplementary Data 11) on the residuals of the Procrustes coordinates data after accounting for centroid size and the scaled phylogeny with the branch-specific average rates obtained from the posterior samples of the Bayesian analyses. Integration analyses are susceptible to sample size differences, and the datasets differ between each type of life cycle (20 paedomorphic, 53 direct-developing and 72 biphasic species). We therefore also assessed the robustness of our

results on the basis of 100 random subsamples of 20 species for the biphasic and direct-developing species that were obtained using the sample function in the base R package v.3.6.1. We compared the average results from these 100 runs with the results from the original analysis.

**Correlation between rates and disparity per module depending on life cycle complexity.** Disparity and rates were quantified for each module depending on the life cycle strategy. Disparity was calculated for each module as the Procrustes variance divided by the number of landmarks per module using `morphol.disparity` in the R package `geomorph`. The evolutionary rates were computed for each element on the basis of a Brownian motion model of evolution using the function `compare.evol.rates` in the `geomorph` R package v.3.1.2. The correlation between the rate of morphological evolution and disparity was assessed using a non-parametric test of Spearman's rank correlation<sup>88</sup> using the `cor.test` function of the `stats` R package v.3.7.0.

**Per-landmark rate and variance.** To assess the correlation between per-landmark Procrustes variance and mean evolutionary rates per bone depending on life cycle, disparity and rates were quantified for each landmark depending on the life cycle strategy (biphasic, direct-developing and paedomorphic datasets). Disparity was calculated for each landmark and semilandmark as the Procrustes variance. The evolutionary rate per landmark and semilandmark was calculated using a modified version of the `compare.evol.rates` function in the `geomorph` R package v.3.1.2 (<https://github.com/rnfelice/hot.dots>)<sup>17,65</sup>. A regression was then performed using the `lm` function from the `stats` R package v.3.7.0 to explore the relationships between disparity and morphological rate per landmark and semilandmark within each bone. To compare the correlation between the within-landmark rate and variance calculated for the different datasets (biphasic, direct-developing and paedomorphic datasets) with the expectation of a Brownian motion model of evolution, we simulated morphological evolution under Brownian motion using the `sim.char` function in the `geiger` R package v.2.0.6.2<sup>89</sup>. The mean variances were estimated after running 100 simulations for each landmark and semilandmark. Finally, a regression of evolutionary rate under Brownian motion on the simulated variance was performed and plotted with its 95% confidence interval.

**Reporting Summary.** Further information on research design is available in the Nature Research Reporting Summary linked to this article.

## Data availability

The scan data that support the findings of this study have been deposited in the Phenome10K repository (<http://phenome10k.org/>) or are already available on MorphoSource and DigiMorph (the URLs and DOIs are available in Supplementary Data 7). The Procrustes coordinates, centroid size, life cycle and microhabitat definitions are available in Supplementary Data 12. The table of module hypotheses used in the modularity analyses is available in Supplementary Data 13. The MCC tree, scaled MCC tree and output of the Bayesian analyses are available at <https://github.com/anjoswami/salamanders>. All other data analysed in this study are included in the Supplementary Information.

## Code availability

The R and BayesTrait codes used in this paper are available at <https://github.com/anjoswami/salamanders>.

Received: 11 September 2019; Accepted: 14 May 2020;

Published online: 22 June 2020

## References

- Hanken, J. Development and evolution in amphibians. *Am. Sci.* **77**, 336–343 (1989).
- Raff, R. A. & Raff, E. C. *Development as an Evolutionary Process* (Alan R. Liss, 1987).
- Bhullar, B.-A. S. et al. Birds have paedomorphic dinosaur skulls. *Nature* **487**, 223–226 (2012).
- Alberch, P. in *Environmental Adaptation and Evolution* (eds Mossakowski, D. & Roth, G.) 19–36 (Gustav Fischer, 1982).
- Roth, G. in *Environmental Adaptation and Evolution* (eds Mossakowski, D. & Roth, G.) 37–48 (Gustav Fischer, 1982).
- Haeckel, E. *Generelle Morphologie der Organismen* Vols. 1 and 2 (G. Reimer, 1866).
- Duméril, A. Reproduction, dans la Ménagerie des Reptiles au Musée d'Histoire Naturelle, des axolotls, batraciens urodèles à branchies persistantes, du Mexique (*Sirenodon mexicanus* vel *Humboldtii*), qui n'avaient encore jamais été vus vivants en Europe. *C. R. Acad. Sci.* **60**, 765–767 (1865).
- Laudet, V. The origins and evolution of vertebrate metamorphosis. *Curr. Biol.* **21**, R726–R737 (2011).
- Mora, C., Tittensor, D. P., Adl, S., Simpson, A. G. B. & Worm, B. How many species are there on Earth and in the ocean? *PLoS Biol.* **9**, e1001127 (2011).

10. McMenamin, S. K. & Parichy, D. M. in *Current Topics in Developmental Biology* Vol. 103 (ed. Shi, Y.-B.) 127–165 (Academic Press, 2013).
11. McMahon, D. P. & Hayward, A. Why grow up? A perspective on insect strategies to avoid metamorphosis. *Ecol. Entomol.* **41**, 505–515 (2016).
12. Rainford, J. L., Hofreiter, M., Nicholson, D. B. & Mayhew, P. J. Phylogenetic distribution of extant richness suggests metamorphosis is a key innovation driving diversification in insects. *PLoS ONE* **9**, e109085 (2014).
13. Rolff, J., Johnston, P. R. & Reynolds, S. Complete metamorphosis of insects. *Philos. Trans. R. Soc. B* **374**, 20190063 (2019).
14. Truman, J. W. & Riddiford, L. M. The evolution of insect metamorphosis: a developmental and endocrine view. *Philos. Trans. R. Soc. B* **374**, 20190070 (2019).
15. Bonner, J. T. *Size and Cycle—an Essay on the Structure of Biology* (Princeton Univ. Press, 1965).
16. Ebenman, B. Niche differences between age classes and intraspecific competition in age-structured populations. *J. Theor. Biol.* **124**, 25–33 (1987).
17. Felice, R. N., Randau, M. & Goswami, A. A fly in a tube: macroevolutionary expectations for integrated phenotypes. *Evolution* **72**, 2580–2594 (2018).
18. Hansen, T. F. Is modularity necessary for evolvability? Remarks on the relationship between pleiotropy and evolvability. *BioSystems* **69**, 83–94 (2003).
19. Drake, A. G. & Klingenberg, C. P. Large-scale diversification of skull shape in domestic dogs: disparity and modularity. *Am. Nat.* **175**, 289–301 (2010).
20. Klingenberg, C. P. Studying morphological integration and modularity at multiple levels: concepts and analysis. *Philos. Trans. R. Soc. B* **369**, 20130249 (2014).
21. Ebenman, B. Evolution in organisms that change their niches during the life cycle. *Am. Nat.* **139**, 990–1021 (1992).
22. Moran, N. A. Adaptation and constraint in the complex life cycles of animals. *Annu. Rev. Ecol. Evol. Syst.* **25**, 573–600 (1994).
23. Wollenberg Valero, K. C. et al. Transcriptomic and macroevolutionary evidence for phenotypic uncoupling between frog life history phases. *Nat. Commun.* **8**, 15213 (2017).
24. Goedert, D. & Calsbeek, R. Experimental evidence that metamorphosis alleviates genomic conflict. *Am. Nat.* **194**, 356–366 (2019).
25. Bonett, R. M. & Blair, A. L. Evidence for complex life cycle constraints on salamander body form diversification. *Proc. Natl Acad. Sci. USA* **114**, 9936–9941 (2017).
26. Vučić, T. et al. Testing the evolutionary constraints of metamorphosis: the ontogeny of head shape in *Triturus* newts. *Evolution* **73**, 1253–1264 (2019).
27. Wake, D. B. & Koo, M. S. Amphibians. *Curr. Biol.* **28**, R1237–R1241 (2018).
28. Ziermann, J. M. in *Heads, Jaws, and Muscles* (eds Ziermann, J., Diaz Jr, R. E. & Diogo, R.) 143–170 (Springer, 2019).
29. Bonett, R. M. in *Evolutionary Developmental Biology* (eds Nuño de la Rosa, L. & Müller, G. B.) 1–14 (Springer, 2018).
30. Bonett, R. M., Chippindale, P. T., Moler, P. E., Wayne, V. D. R. & Wake, D. B. Evolution of gigantism in amphiumid salamanders. *PLoS ONE* **4**, e5615 (2009).
31. Bonett, R. M., Steffen, M. A., Lambert, S. M., Wiens, J. J. & Chippindale, P. T. Evolution of paedomorphosis in plethodontid salamanders: ecological correlates and re-evolution of metamorphosis. *Evolution* **68**, 466–482 (2013).
32. Chippindale, P. T., Bonett, R. M., Baldwin, A. S. & Wiens, J. J. Phylogenetic evidence for a major reversal of life-history evolution in plethodontid salamanders. *Evolution* **58**, 2809–2822 (2004).
33. Ledbetter, N. M. & Bonett, R. M. Terrestriality constrains salamander limb diversification: implications for the evolution of pentadactyly. *J. Evol. Biol.* **32**, 642–652 (2019).
34. Blankers, T., Adams, D. C. & Wiens, J. J. Ecological radiation with limited morphological diversification in salamanders. *J. Evol. Biol.* **25**, 634–646 (2012).
35. Hanken, J. & Hall, B. K. *The Skull: Patterns of Structural and Systematic Diversity* Vol. 2 (Univ. of Chicago Press, 1993).
36. Vassilieva, A. B., Lai, J.-S., Yang, S.-F., Chang, Y.-H. & Poyarkov, N. A. J. Development of the bony skeleton in the Taiwan salamander, *Hynobius formosanus* Maki, 1922 (Caudata: Hynobiidae): heterochronies and reductions. *Vert. Zool.* **65**, 117–130 (2015).
37. Truman, J. W. & Riddiford, L. M. The origins of insect metamorphosis. *Nature* **401**, 447–452 (1999).
38. Taylor, M. A. How tetrapods feed in water: a functional analysis by paradigm. *Zool. J. Linn. Soc.* **91**, 171–195 (1987).
39. Schwenk, K. *Feeding: Form, Function, and Evolution in Tetrapod Vertebrates* (Academic Press, 2000).
40. Bels, V. & Whishaw, I. Q. *Feeding in Vertebrates: Evolution, Morphology, Behavior, Biomechanics* (Springer, 2019).
41. Duellman, W. E. & Trueb, L. *Biology of Amphibians* (McGraw-Hill, 1986).
42. Johnson, C. K. & Voss, S. R. Salamander paedomorphosis: linking thyroid hormone to life history and life cycle evolution. *Curr. Top. Dev. Biol.* **103**, 229–257 (2013).
43. Wilbur, H. M. & Collins, J. P. Ecological aspects of amphibian metamorphosis. *Science* **182**, 1305–1314 (1973).
44. Clavel, J. & Morlon, H. Accelerated body size evolution during cold climatic periods in the Cenozoic. *Proc. Natl Acad. Sci. USA* **114**, 4183–4188 (2017).
45. Botero, C. A., Dor, R., McCain, C. M. & Safran, R. J. Environmental harshness is positively correlated with intraspecific divergence in mammals and birds. *Mol. Ecol.* **23**, 259–268 (2014).
46. Laurin, M. Assessment of modularity in the urodele skull: an exploratory analysis using ossification sequence data. *J. Exp. Zool. B* **322**, 567–585 (2014).
47. Ivanović, A. & Kalezić, M. L. Testing the hypothesis of morphological integration on a skull of a vertebrate with a biphasic life cycle: a case study of the alpine newt. *J. Exp. Zool. B* **314B**, 527–538 (2010).
48. Kerney, R. R., Blackburn, D. C., Müller, H. & Hanken, J. Do larval traits re-evolve? Evidence from the embryogenesis of a direct-developing salamander, *Plethodon cinereus*. *Evolution* **66**, 252–262 (2012).
49. Bon, M., Bardua, C., Goswami, A. & Fabre, A.-C. Cranial integration in the fire salamander, *Salamandra salamandra* (Caudata: Salamandridae). *Biol. J. Linn. Soc.* **130**, 178–194 (2020).
50. Wake, D. B. Comparative osteology and evolution of the lungless salamanders, family Plethodontidae. *Mem. Calif. Acad. Sci.* **4**, 1–111 (1966).
51. Reilly, S. M. Ontogeny of cranial ossification in the eastern newt, *Notophthalmus viridescens* (Caudata: Salamandridae), and its relationship to metamorphosis and neoteny. *J. Morphol.* **188**, 315–326 (1986).
52. Ultsch, G. R. & Duke, J. T. Gas exchange and habitat selection in the aquatic salamanders *Necturus maculosus* and *Cryptobranchus alleganiensis*. *Oecologia* **83**, 250–258 (1990).
53. Hanken, J. Life-history and morphological evolution. *J. Evol. Biol.* **5**, 549–557 (1992).
54. Dinis, M. & Velo-Antón, G. How little do we know about the reproductive mode in the north African salamander, *Salamandra algira*? Pueriparity in divergent mitochondrial lineages of *S. a. tingitana*. *Amphib. Reptil.* **38**, 540–546 (2017).
55. Kraemer, A. C. & Adams, D. C. Predator perception of Batesian mimicry and conspicuousness in a salamander. *Evolution* **68**, 1197–1206 (2014).
56. Heiss, E. & Grell, J. Same but different: aquatic prey capture in paedomorphic and metamorphic alpine newts. *Zool. Lett.* **5**, 5–24 (2019).
57. Bookstein, F. L. Landmark methods for forms without landmarks: morphometrics of group differences in outline shape. *Med. Image Anal.* **1**, 225–243 (1997).
58. Gunz, P., Mitteroecker, P. & Bookstein, F. L. in *Modern Morphometrics in Physical Anthropology* (ed. Slice, D. E.) 73–98 (Springer, 2005).
59. Bardua, C., Felice, R. N., Watanabe, A., Fabre, A. C. & Goswami, A. A practical guide to sliding and surface semilandmarks in morphometric analyses. *Integr. Organism. Biol.* **1**, 1–34 (2019).
60. Parr, W. C. et al. Toward integration of geometric morphometrics and computational biomechanics: new methods for 3D virtual reconstruction and quantitative analysis of finite element models. *J. Theor. Biol.* **301**, 1–14 (2012).
61. Wiley, D. F. et al. Evolutionary morphing. In *Proc. IEEE Visualization 2005 (VIS'05) 23–28 October 2005* 431–438 (IEEE, 2005).
62. Dumont, M. et al. Do functional demands associated with locomotor habitat, diet, and activity pattern drive skull shape evolution in musteloid carnivorans? *Biol. J. Linn. Soc.* **117**, 858–878 (2016).
63. Fabre, A. C., Marigo, J., Granatosky, M. C. & Schmitt, D. Functional associations between support use and forelimb shape in strepsirrhines and their relevance to inferring locomotor behavior in early primates. *J. Hum. Evol.* **108**, 11–30 (2017).
64. Felice, R. N. & Goswami, A. Developmental origins of mosaic evolution in the avian cranium. *Proc. Natl Acad. Sci. USA* **115**, 555–560 (2018).
65. Watanabe, A. et al. Ecomorphological diversification in squamates from conserved pattern of cranial integration. *Proc. Natl Acad. Sci. USA* **116**, 14688–14697 (2019).
66. Bardua, C., Wilkinson, M., Gower, D. J., Sherratt, E. & Goswami, A. Morphological evolution and modularity of the caecilian skull. *BMC Evol. Biol.* **19**, 30 (2019).
67. Marshall, A. F. et al. High-density three-dimensional morphometric analyses support conserved static (intraspecific) modularity in caecilian (Amphibia: Gymnophiona) crania. *Biol. J. Linn. Soc.* **126**, 721–742 (2019).
68. Botton-Divet, L., Cornette, R., Fabre, A.-C., Herrel, A. & Houssaye, A. Morphological analysis of long bones in semi-aquatic mustelids and their terrestrial relatives. *Integr. Comp. Biol.* **56**, 1298–1309 (2016).
69. Schlager, S. in *Statistical Shape and Deformation Analysis* (eds Zheng, G. et al.) 217–256 (Academic Press, 2017).
70. Klingenberg, C. Novelty and “homology-free” morphometrics: what’s in a name? *Evol. Biol.* **35**, 186–190 (2008).
71. Cardini, A. Lost in the other half: improving accuracy in geometric morphometric analyses of one side of bilaterally symmetric structures. *Syst. Biol.* **65**, 1096–1106 (2016).
72. Jetz, W. & Pyron, R. A. The interplay of past diversification and evolutionary isolation with present imperilment across the amphibian tree of life. *Nat. Ecol. Evol.* **2**, 850–858 (2018).
73. Drummond, A. J. & Rambaut, A. BEAST: Bayesian evolutionary analysis by sampling trees. *BMC Evol. Biol.* **7**, 214 (2007).

74. Heled, J. & Bouckaert, R. R. Looking for trees in the forest: summary tree from posterior samples. *BMC Evol. Biol.* **13**, 221 (2013).
75. Parra-Olea, G. et al. Biology of tiny animals: three new species of minute salamanders (Plethodontidae: *Thorius*) from Oaxaca, Mexico. *PeerJ* **4**, e2694 (2016).
76. Wang, B. et al. Phylogenetic surveys on the newt genus *Tylototriton* sensu lato (Salamandridae, Caudata) reveal cryptic diversity and novel diversification promoted by historical climatic shifts. *PeerJ* **6**, e4384 (2018).
77. Collyer, M. L. & Adams, D. C. RRPP: Linear model evaluation with randomized residuals in a permutation procedure. R package version 3.1.2 <https://cran.r-project.org/web/packages/RRPP> (2019).
78. Collyer, M. L. & Adams, D. C. An R package for fitting linear models to high-dimensional data using residual randomization. *Methods Ecol. Evol.* **9**, 1772–1779 (2018).
79. Revell, L. J. Phytools: an R package for phylogenetic comparative biology (and other things). *Methods Ecol. Evol.* **3**, 217–223 (2012).
80. Zelditch, M. L., Swiderski, D. L., Sheets, H. D. & Fink, W. L. *Geometric Morphometrics for Biologists: A Primer* (Elsevier/Academic Press, 2012).
81. Venditti, C., Meade, A. & Pagel, M. Multiple routes to mammalian diversity. *Nature* **479**, 393–396 (2011).
82. Gelman, A. & Rubin, D. B. Inference from iterative simulation using multiple sequences. *Stat. Sci.* **7**, 457–472 (1992).
83. Yang, Z. *Computational Molecular Evolution* (Oxford Univ. Press, 2006).
84. Akaike, H. in *Proceedings of the 2nd International Symposium on Information Theory* (eds Petrov, B. N. & Csaki, F.) 267–281 (Akademiai Kiado, 1973).
85. Goswami, A. & Finarelli, J. A. EMLI: a maximum likelihood approach to the analysis of modularity. *Evolution* **70**, 1622–1637 (2016).
86. Adams, D. C. Evaluating modularity in morphometric data: challenges with the RV coefficient and a new test measure. *Methods Ecol. Evol.* **7**, 565–572 (2016).
87. Adams, D. C. & Felice, R. N. Assessing phylogenetic morphological integration and trait covariation in morphometric data using evolutionary covariance matrices. *PLoS ONE* **9**, e9433 (2014).
88. Spearman, C. The proof and measurement of association between two things. *Am. J. Psychol.* **15**, 72–101 (1904).
89. Pennell, M. W. et al. geiger v2.0: an expanded suite of methods for fitting macroevolutionary models to phylogenetic trees. *Bioinformatics* **30**, 2216–2218 (2014).

## Acknowledgements

We thank A.-M. Ohler at the MNHN, the herpetology group at the NHM and N. Fröbisch, K. Mahlow and F. Glöckler at the Museum für Naturkunde. We also thank V. Fernandez and B. Clark for providing training for CT scanning at the NHM and J. Maisano for giving access to CT scans from DigiMorph.org on the NSF grant nos. EF-0334952, IIS-9874781 and IIS-0208675. This work was funded by the European Research Council (grant no. STG-2014–637171 to A.G.) and by a Synthesis (grant no. FR-TAF-5583 to C.B.). This research received support from the US National Science Foundation (oVert TCN; NSF grant no. DBI-1701714) and from the SYNTHESYS Project (<http://www.SYNTHESYS.info/>), which is financed by European Community Research Infrastructure Action under the FP7 Integrating Activities Programme. We thank B. Poole for help with the analyses.

## Author contributions

A.-C.F. and A.G. conceived and designed the study. A.-C.F., C.B., M.B., D.C.B., J.B. and E.L.S. acquired and processed the CT data. A.-C.F. acquired the geometric morphometric data. A.-C.F., C.B., J.C. and R.N.F. conducted the analyses. A.-C.F. wrote the initial draft of the manuscript. C.B., M.B., J.C., R.N.F., D.C.B., J.W.S., J.B., E.L.S. and A.G. contributed to the interpretation of the data and to the editing of subsequent drafts of the manuscript.

## Competing interests

The authors declare no competing interests.

## Additional information

**Extended data** is available for this paper at <https://doi.org/10.1038/s41559-020-1225-3>.

**Supplementary information** is available for this paper at <https://doi.org/10.1038/s41559-020-1225-3>.

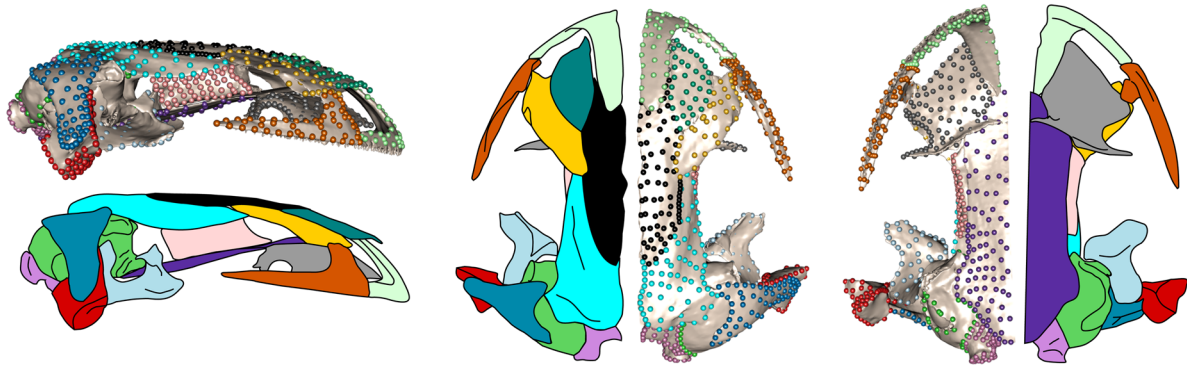
**Correspondence and requests for materials** should be addressed to A.-C.F.

**Reprints and permissions information** is available at [www.nature.com/reprints](http://www.nature.com/reprints).

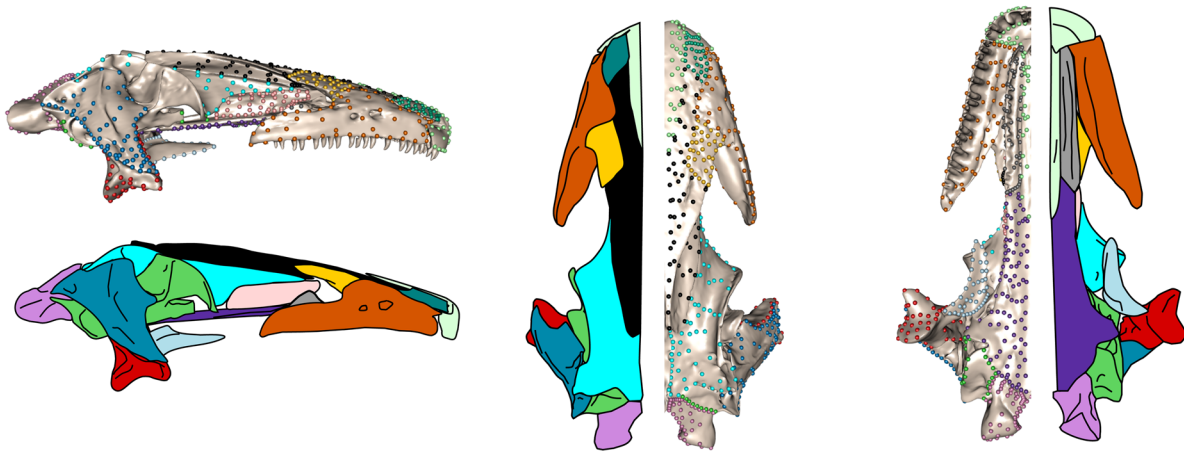
**Publisher's note** Springer Nature remains neutral with regard to jurisdictional claims in published maps and institutional affiliations.

© The Author(s), under exclusive licence to Springer Nature Limited 2020

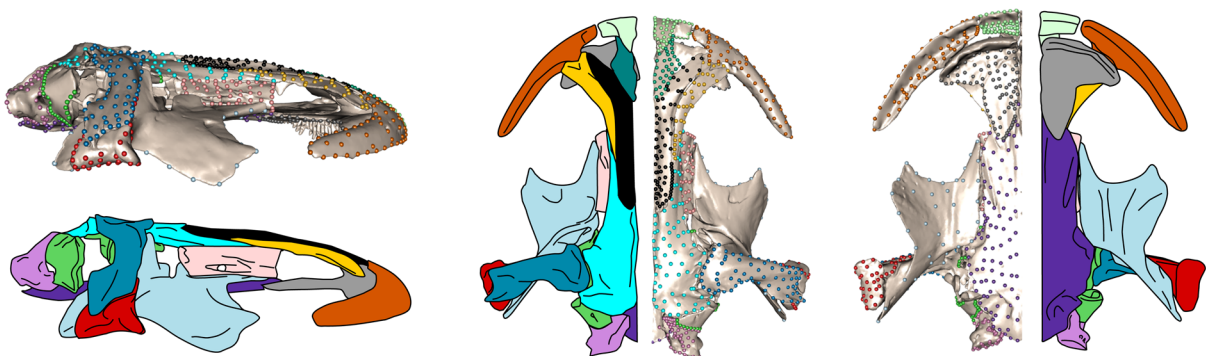
**Ambystomatidae**



**Amphiumidae**



**Cryptobranchidae**

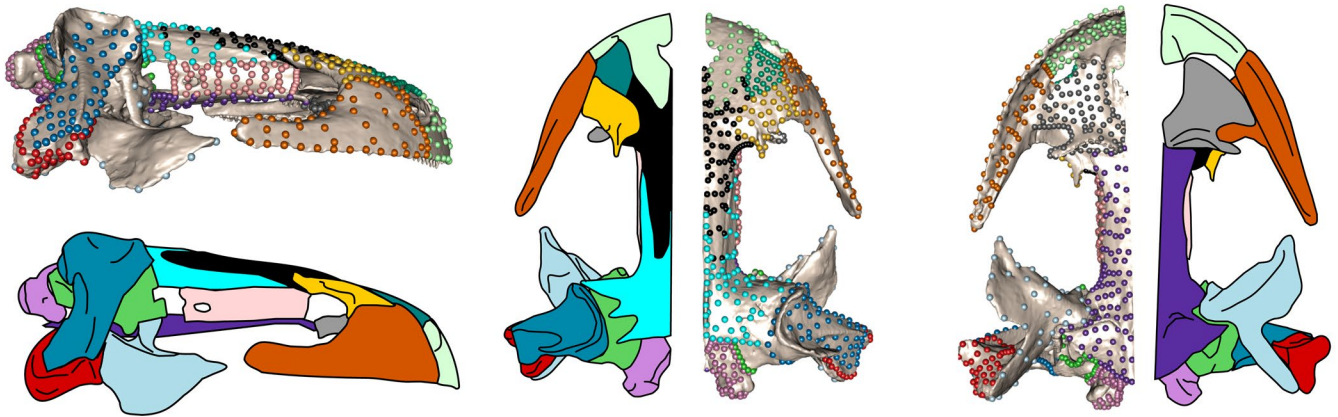


**Bone colors:**

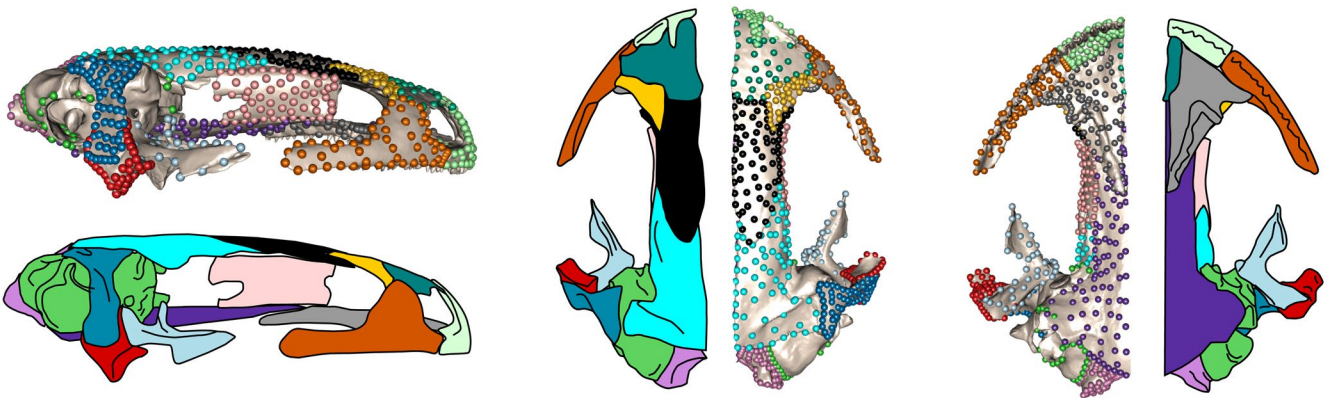
■ Frontal	■ Occipital	■ Parietal	■ Parasphenoid	■ Squamosal
■ Maxilla	■ Orbitosphenoid	■ Premaxilla	■ Pterygoid	■ Vomer
■ Nasal	■ Otic	■ Prefrontal	■ Quadrate	

**Extended Data Fig. 1 | Landmarks used to quantify cranial shape variation in Ambystomatidae, Amphiumidae and Cryptobranchidae.** Landmarks used to quantify cranial shape variation in Ambystomatidae (*Ambystoma tigrinum*), Amphiumidae (*Amphiuma means*) and Cryptobranchidae (*Cryptobranchus alleganiensis*). Sliding landmarks that describe the 14 bones and 19 regions of the cranium used in all shape analyses. From the left to the right: lateral, dorsal and ventral views of the cranium.

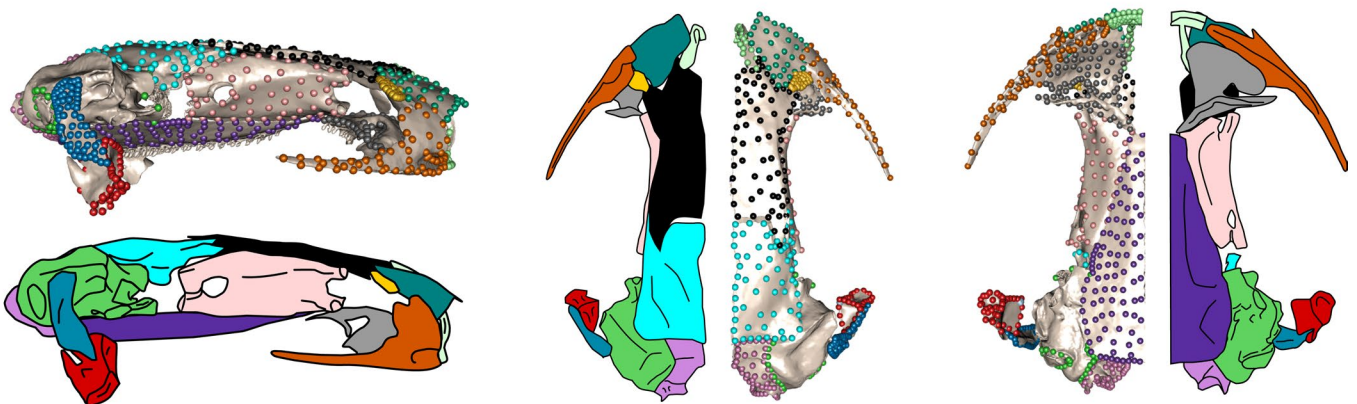
## Dicamptodontidae



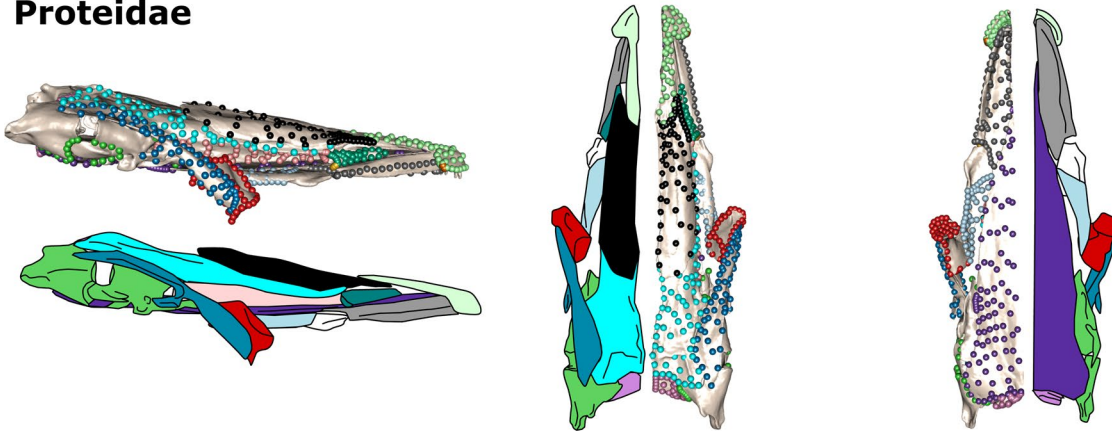
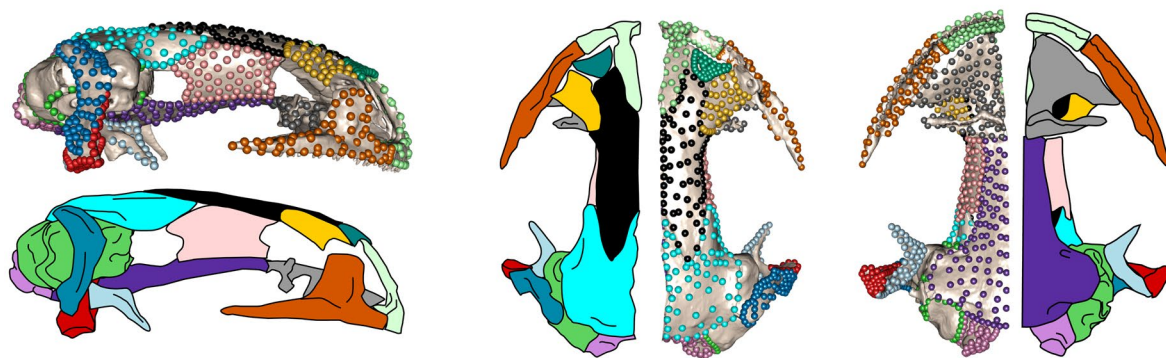
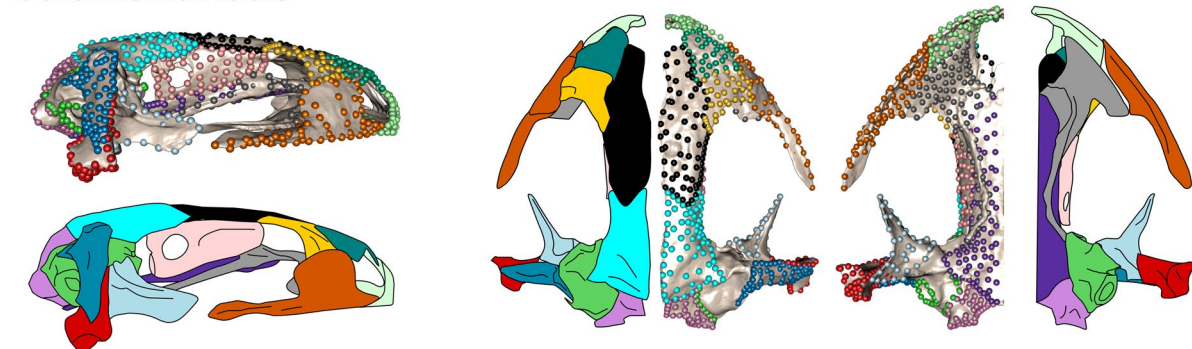
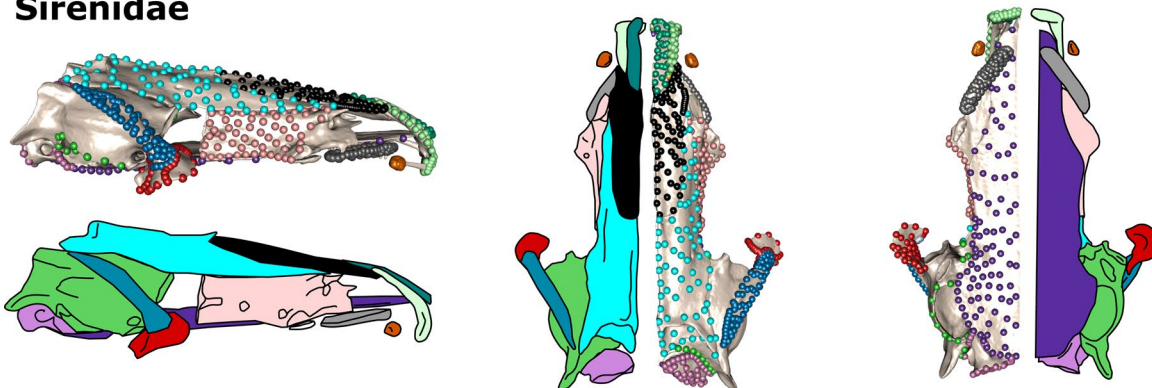
## Hynobiidae



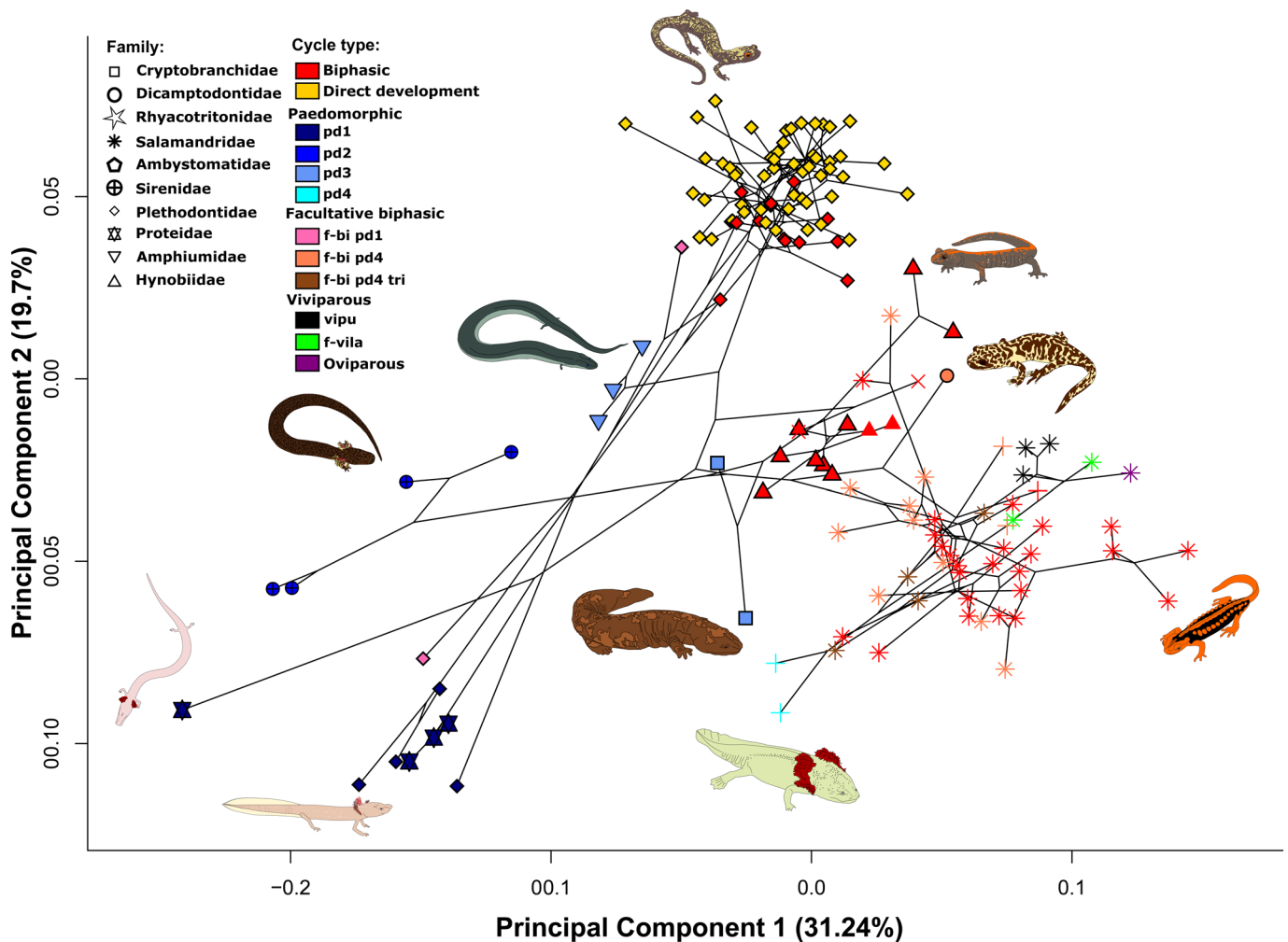
## Plethodontidae



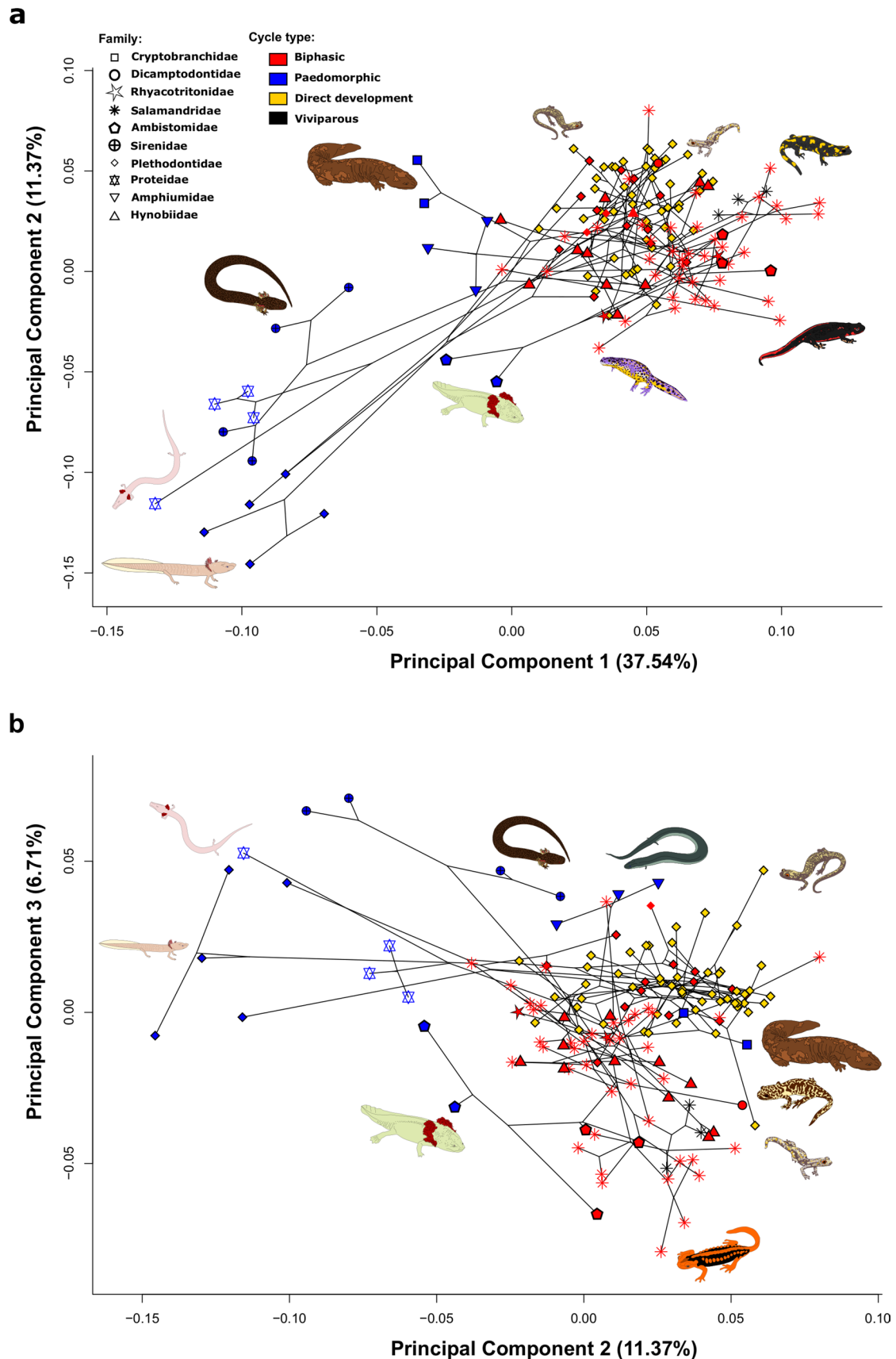
**Extended Data Fig. 2 | Landmarks used to quantify cranial shape variation in Dicamptodontidae, Hynobiidae and Plethodontidae.** Landmarks used to quantify cranial shape variation in Dicamptodontidae (*Dicamptodon ensatus*), Hynobiidae (*Hynobius leechi*) and Plethodontidae (*Bolitoglossa salvinii*). Sliding landmarks that describe the 14 bones and 19 regions of the cranium used in all shape analyses. From the left to the right: lateral, dorsal and ventral views of the cranium. See colors key in Extended Data Fig. 1.

**Proteidae****Rhyacotritonidae****Salamandridae****Sirenidae**

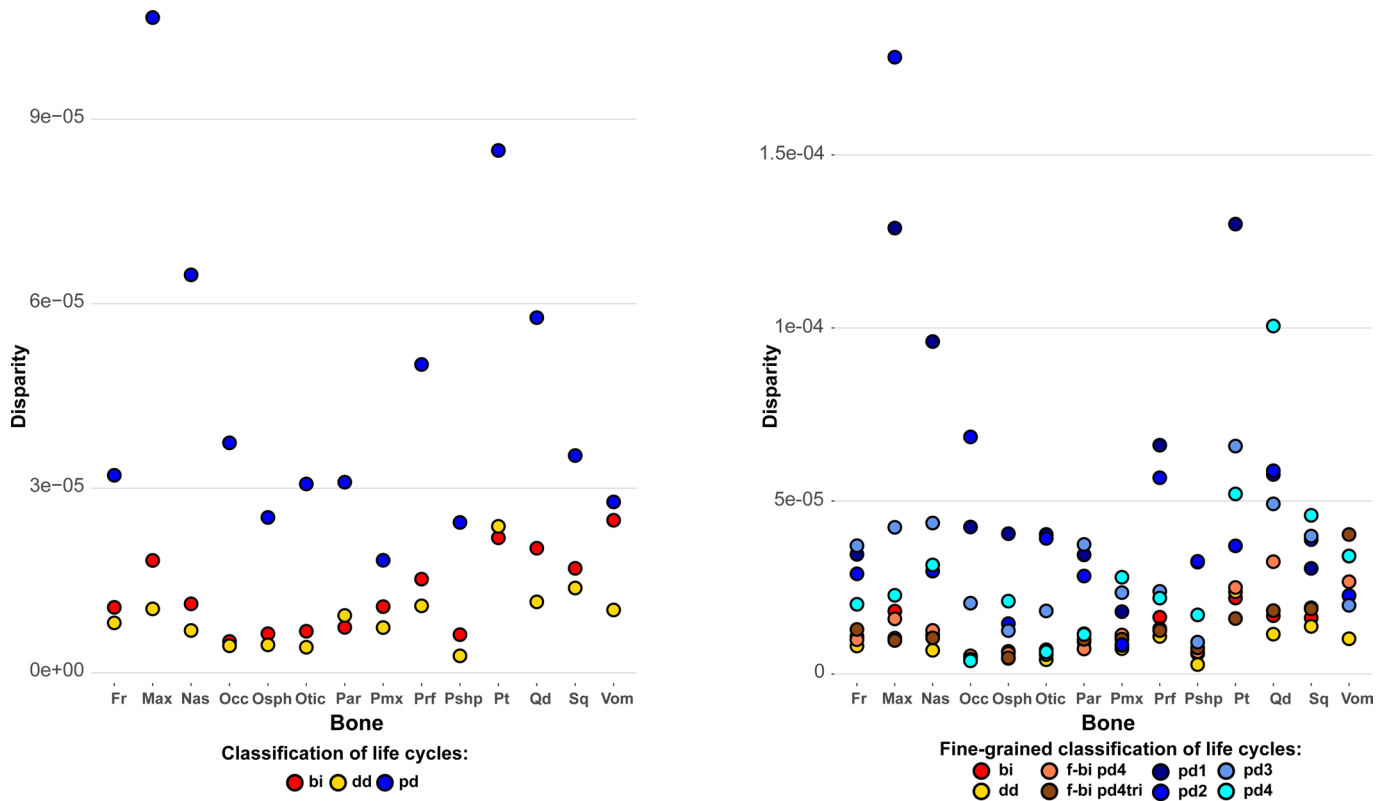
**Extended Data Fig. 3 | Landmarks used to quantify cranial shape variation in Proteidae, Rhyacotritonidae, Salamandridae and Sirenidae.** Landmarks used to quantify cranial shape variation in Proteidae (*Proteus anguinus*), Rhyacotritonidae (*Rhyacotriton variegatus*), Salamandridae (*Salamandra salamandra*) and Sirenidae (*Siren intermedia*). Sliding landmarks that describe the 14 bones and 19 regions of the cranium used in all shape analyses. From the left to the right: lateral, dorsal and ventral views of the cranium. See colors key in Extended Data Fig. 1.



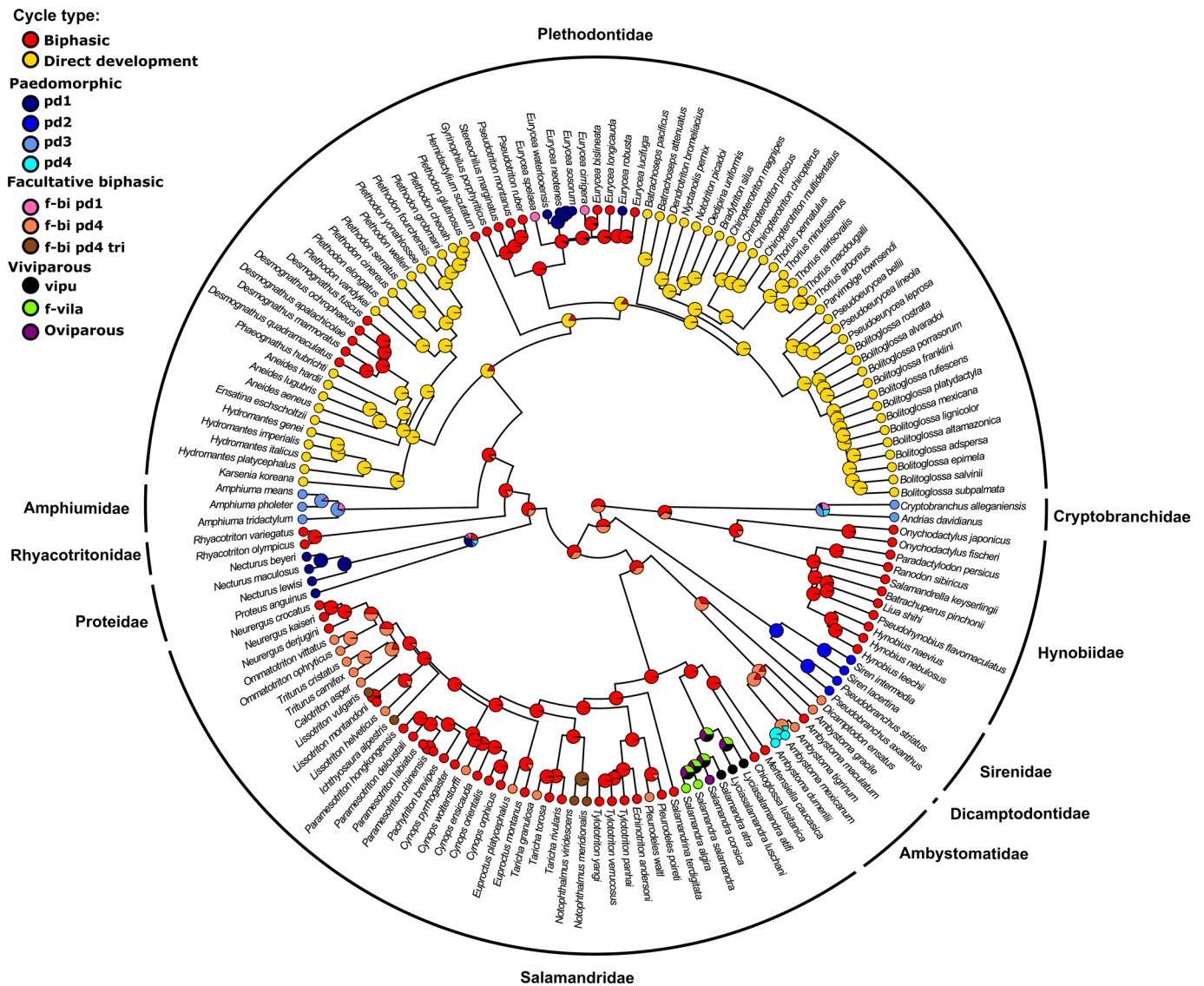
**Extended Data Fig. 4 | Phylomorphospace illustrating the first two principal components of cranial shape across Caudata depending on fine-grained classifications of life cycle.** Phylomorphospace illustrating the first two principal components of cranial shape across Caudata. Symbols indicate family-level clade and colours represent fine-grained classifications of life cycle. Abbreviations are as follows: f-bi pd1 indicates facultative biphasic species, as some populations can be paedomorphic in these species. When they are paedomorphic they display external gills, gill slits, a tail fin, no eyelids, no maxillary bones, no septomaxilla and no prefrontal; f-bi pd4 indicates facultative biphasic species, as some populations can be paedomorphic in these species. When they are paedomorphic they display external gills, gill slits, tail fin, no eyelids, no septomaxilla and with maxillary and prefrontal bones developing before adulthood; f-bi pd4tri indicates species that are triphasic; pd1 indicates paedomorphic species with external gills, gill slits, tail fin, no eyelids, no maxillary bones, no septomaxilla and no prefrontal; pd2 indicates paedomorphic species with external gills, gill slits, tail fin, no eyelids, no septomaxilla, no prefrontal and with maxillary bones developing before adulthood; pd3 indicates paedomorphic species without external gills but with gill slits, tail fin, no eyelids, no septomaxilla and with maxillary and prefrontal bones developing before adulthood; pd4 indicates paedomorphic species with external gills, gill slits, tail fin, no eyelids, no septomaxilla and with maxillary and prefrontal bones developing before adulthood; vipu indicates strictly puereparate viviparous species; f-vila indicates facultative larviparous viviparous species; ovi indicates oviparous species.



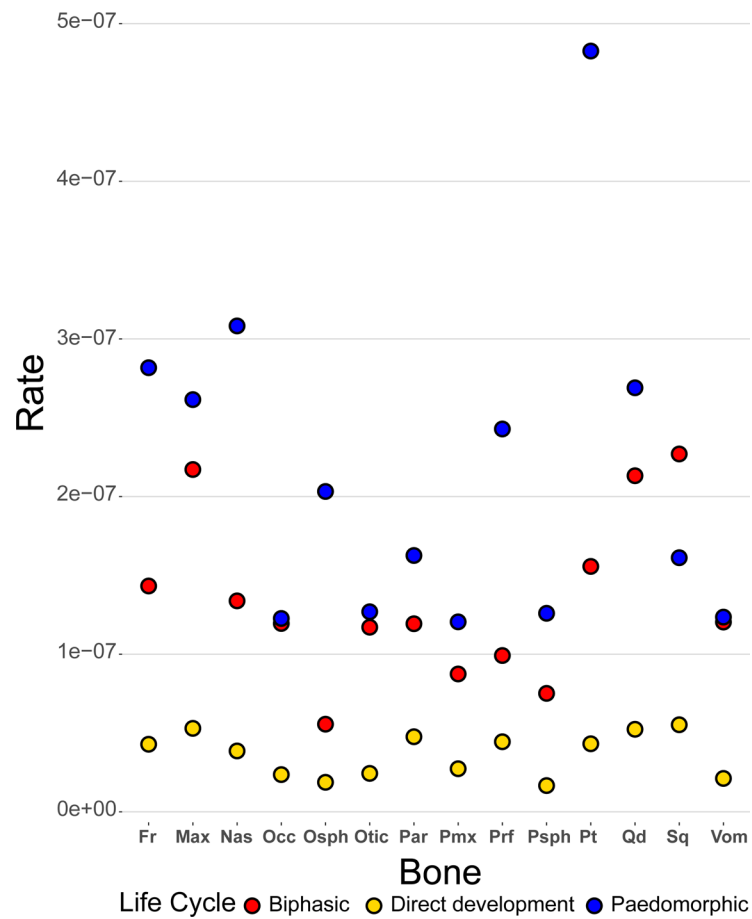
**Extended Data Fig. 5 | Phylogenetic principal component on cranial shape depending on life cycle.** Phylomorphospace on skull shape of Caudata. a) Phylomorphospace of the first two phylogenetic principal component scores showing the skull shape distribution of Caudata. b) Phylomorphospace of the second and third phylogenetic principal component scores showing the skull shape distribution of Caudata. Data point shapes are coded by family group and colors represent life cycles, as indicated by the key.



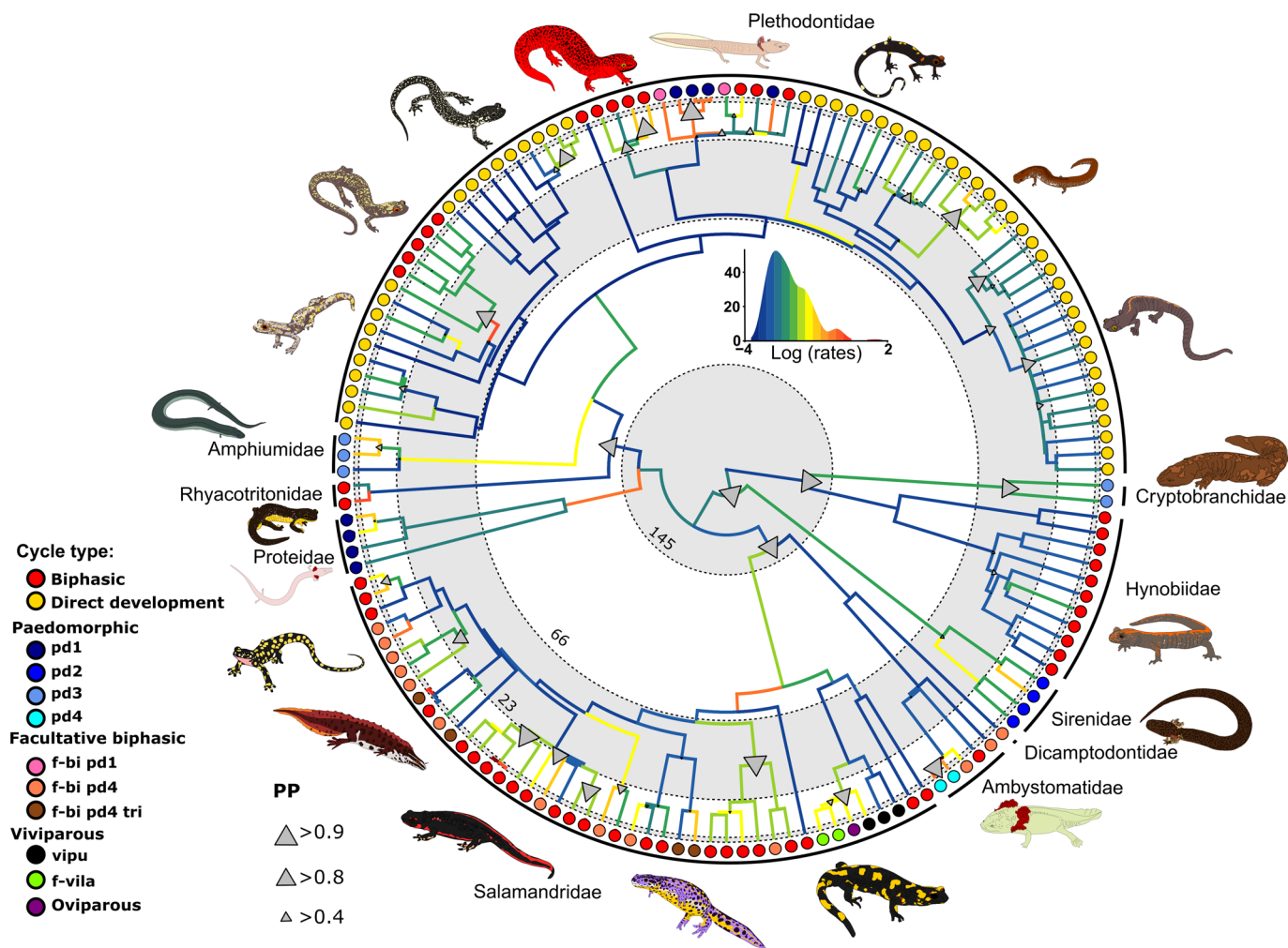
**Extended Data Fig. 6 | Disparity depending on life cycle and on fine-grained classifications corrected by the number of landmarks per bone.** Disparity per life cycle and on fine-grained classifications corrected by the number of landmarks per bone. Left: analyses were run on the whole data set and excluded the strictly viviparous species for the classification of life cycles. Right: these analyses were run on the whole data set excluding the strictly viviparous (f-vila as  $n=2$  and vipu as  $n=2$ ), oviparous ( $n=1$ ) and facultative biphasic pd1 (f-bi pd1 as  $n=2$ ) species for the classification of life cycles. Abbreviations are as follows: f-bi pd1 indicates facultative biphasic species, as some populations can be paedomorphic in these species. When they are paedomorphic they display external gills, gill slits, a tail fin, no eyelids, no maxillary bones, no septomaxilla and no prefrontal; f-bi pd4 indicates facultative biphasic species, as some populations can be paedomorphic in these species. When they are paedomorphic they display external gills, gill slits, tail fin, no eyelids, no septomaxilla and with maxillary and prefrontal bones developing before adulthood; f-bi pd4tri indicates species that are triphasic; pd1 indicates paedomorphic species with external gills, gill slits, tail fin, no eyelids, no maxillary bones, no septomaxilla and no prefrontal; pd2 indicates paedomorphic species with external gills, gill slits, tail fin, no eyelids, no septomaxilla, no prefrontal and with maxillary bones developing before adulthood; pd3 indicates paedomorphic species without external gills but with gill slits, tail fin, no eyelids, no septomaxilla and with maxillary and prefrontal bones developing before adulthood; pd4 indicates paedomorphic species with external gills, gill slits, tail fin, no eyelids, no septomaxilla and with maxillary and prefrontal bones developing before adulthood; vipu indicates strictly puereparate viviparous species; f-vila indicates facultative larviparous species; ovi indicates oviparous species.



**Extended Data Fig. 7 | Evolution of life cycles in Caudata using fine-grained classifications.** Evolution of life cycles in Caudata using fine-grained classifications. Ancestral state estimation using a re-rooting method using the symmetric rate model (best model following results of the AIC, Supplementary Table 5). Abbreviations are as follows: f-bi pd1 indicates facultative biphasic species, as some populations can be paedomorphic in these species. When they are paedomorphic they display external gills, gill slits, a tail fin, no eyelids, no maxillary bones, no septomaxilla and no prefrontal; f-bi pd4 indicates facultative biphasic species, as some populations can be paedomorphic in these species. When they are paedomorphic they display external gills, gill slits, tail fin, no eyelids, no septomaxilla and with maxillary and prefrontal bones developing before adulthood; f-bi pd4tri indicates species that are triphasic; pd1 indicates paedomorphic species with external gills, gill slits, tail fin, no eyelids, no maxillary bones, no septomaxilla and no prefrontal; pd2 indicates paedomorphic species with external gills, gill slits, tail fin, no eyelids, no septomaxilla, no prefrontal and with maxillary bones developing before adulthood; pd3 indicates paedomorphic species without external gills but with gill slits, tail fin, no eyelids, no septomaxilla and with maxillary and prefrontal bones developing before adulthood; pd4 indicates paedomorphic species with external gills, gill slits, tail fin, no eyelids, no septomaxilla and with maxillary and prefrontal bones developing before adulthood; vipu indicates strictly puereparate viviparous species; f-vila indicates facultative larviparous species; ovi indicates oviparous species.



**Extended Data Fig. 8 | Rate of evolution per life cycle.** Rate of evolution per life cycle. These analyses were run on the whole data set excluding the strictly viviparous species.



**Extended Data Fig. 9 | Evolutionary rates and rate shifts for cranial shape in Caudata.** Evolutionary rates and rate shifts for cranial shape in Caudata. Colour gradients on branches indicate the rate of shape evolution with warmer colours corresponding to a higher rate and cooler colours to a lower one. Grey triangles indicate the stem branch of clades with support for whole-clade shifts in evolutionary rate. Posterior probabilities (PP) of rate shifts are indicated by the relative size of the triangles (see Extended Data Fig. 10). Frequencies of the log-transformed rates of cranial shape evolution are indicated by the distribution plot. Rates and shift were estimated using BayesTraitsV3 using a variable-rates Brownian motion model. Times in the tree are indicated in millions of years (Ma). Abbreviations are as follows: f-bi pd1 indicates facultative biphasic species, as some populations can be paedomorphic in these species. When they are paedomorphic they display external gills, gill slits, a tail fin, no eyelids, no maxillary bones, no septomaxilla and no prefrontal; f-bi pd4 indicates facultative biphasic species, as some populations can be paedomorphic in these species. When they are paedomorphic they display external gills, gill slits, tail fin, no eyelids, no septomaxilla and with maxillary and prefrontal bones developing before adulthood; f-bi pd4tri indicates species that are triphasic; pd1 indicates paedomorphic species with external gills, gill slits, tail fin, no eyelids, no maxillary bones, no septomaxilla and no prefrontal; pd2 indicates paedomorphic species with external gills, gill slits, tail fin, no eyelids, no septomaxilla, no prefrontal and with maxillary bones developing before adulthood; pd3 indicates paedomorphic species without external gills but with gill slits, tail fin, no eyelids, no septomaxilla and with maxillary and prefrontal bones developing before adulthood; pd4 indicates paedomorphic species with external gills, gill slits, tail fin, no eyelids, no septomaxilla and with maxillary and prefrontal bones developing before adulthood; vipu indicates strictly puereparate viviparous species; f-vila indicates facultative larviparate viviparous species; ovi indicates oviparous species.



## Reporting Summary

Nature Research wishes to improve the reproducibility of the work that we publish. This form provides structure for consistency and transparency in reporting. For further information on Nature Research policies, see our [Editorial Policies](#) and the [Editorial Policy Checklist](#).

### Statistics

For all statistical analyses, confirm that the following items are present in the figure legend, table legend, main text, or Methods section.

n/a Confirmed

- The exact sample size ( $n$ ) for each experimental group/condition, given as a discrete number and unit of measurement
- A statement on whether measurements were taken from distinct samples or whether the same sample was measured repeatedly
- The statistical test(s) used AND whether they are one- or two-sided  
*Only common tests should be described solely by name; describe more complex techniques in the Methods section.*
- A description of all covariates tested
- A description of any assumptions or corrections, such as tests of normality and adjustment for multiple comparisons
- A full description of the statistical parameters including central tendency (e.g. means) or other basic estimates (e.g. regression coefficient) AND variation (e.g. standard deviation) or associated estimates of uncertainty (e.g. confidence intervals)
- For null hypothesis testing, the test statistic (e.g.  $F$ ,  $t$ ,  $r$ ) with confidence intervals, effect sizes, degrees of freedom and  $P$  value noted  
*Give  $P$  values as exact values whenever suitable.*
- For Bayesian analysis, information on the choice of priors and Markov chain Monte Carlo settings
- For hierarchical and complex designs, identification of the appropriate level for tests and full reporting of outcomes
- Estimates of effect sizes (e.g. Cohen's  $d$ , Pearson's  $r$ ), indicating how they were calculated

*Our web collection on [statistics for biologists](#) contains articles on many of the points above.*

### Software and code

Policy information about [availability of computer code](#)

#### Data collection

Avizo Lite 9 (FEI Visualization Sciences Group, Burlington, MA, USA) was used to segment and export the skull reconstructions of each specimen as PLY files. All the PLY files were imported into Geomagic Wrap (3D Systems, Rock Hill, South Carolina, USA) in order to clean, repair and decimate the meshes prior to the landmarking procedure. All the landmarks and semi-landmarks of curves were collected using the software package IDAV Landmark (<http://graphics.idav.ucdavis.edu/research/EvoMorph>). All the surface sliding semilandmarks were obtained using a semi-automated approach in the 'Morpho' package v2.5.1 in R version 3.5.1. A hemispheric template mesh were created using a 360 x 360 uniform-vertex sphere created in Meshlab (<http://www.meshlab.net/>) and modified in Blender (Stitching Blender Foundation, Amsterdam, Netherlands).

#### Data analysis

R Studio using the software version 3.5.1:  
The landmarks and semilandmarks were mirrored using the mirrorfill function in the 'paleomorph' R package v0.1.4.  
Phylogenetic principal component analysis on which the phylogeny was mapped using the function phylomorphospace from the 'phytools' R package v0.6-99.  
Phylogenetic analysis of variance (MANOVA) using the function procD.pgls, Brownian motion BM model of evolution using the function compare.multi.evol.rates, morphological disparities for each life cycle strategy (biphasic, paedomorphic, and direct development) we used the function morphol.disparity, CR was estimated using the modularity.test function, residuals of the Procrustes coordinates data after accounting for size and phylogeny were obtained using procD.pgls function, evolutionary rates were computed for each element based on a BM model of evolution using the function compare.evol.rates from the 'geomorph' R package v3.1.2  
Effective sample size of the posterior samples (ESS>100) was assessed using the effectiveSize function and convergence of the chains was assessed using Gelman and Rubin's convergence diagnostic(function gelman.diag); both functions are implemented in the R package 'coda' v0.19-3.  
Modularity using the function EMMLi from the 'EMMLi' R package v 0.0.3.  
A linear regression was performed using the lm function of the 'stats' R package v3.7.0  
Expectation of a Brownian motion model of evolution, we simulated morphological evolution under BM using the sim.char function in the 'geiger' R package v2.0.6.2

The results of the bayesian analyses were summarized by the branch-specific average rate and the posterior probability of rate shifts, both estimated from the posterior samples using the `rjpp` and the `plotShift` functions in the 'btrtools' R package (<https://github.com/hferg/btrtools/tree/master/R>) using the algorithm implemented in the `rerootingMethod` function in `phytools` v0.6-99.

For manuscripts utilizing custom algorithms or software that are central to the research but not yet described in published literature, software must be made available to editors and reviewers. We strongly encourage code deposition in a community repository (e.g. GitHub). See the Nature Research [guidelines for submitting code & software](#) for further information.

## Data

Policy information about [availability of data](#)

All manuscripts must include a [data availability statement](#). This statement should provide the following information, where applicable:

- Accession codes, unique identifiers, or web links for publicly available datasets
- A list of figures that have associated raw data
- A description of any restrictions on data availability

Scan data that support the findings of this study have been deposited in the Phenome10K repository (<http://phenome10k.org/>) or are already available on MorphoSource and DigiMorph. All other data analysed in this study are included in Supplemental Information and are also available at <https://github.com/anjosgswami/salamanders>.

## Field-specific reporting

Please select the one below that is the best fit for your research. If you are not sure, read the appropriate sections before making your selection.

- Life sciences       Behavioural & social sciences       Ecological, evolutionary & environmental sciences

For a reference copy of the document with all sections, see [nature.com/documents/nr-reporting-summary-flat.pdf](https://www.nature.com/documents/nr-reporting-summary-flat.pdf)

## Ecological, evolutionary & environmental sciences study design

All studies must disclose on these points even when the disclosure is negative.

### Study description

We reconstruct the evolution of the salamander skull using high-density geometric morphometric data from 148 species spanning their full phylogenetic, ecological, and developmental diversity. We quantify skull shape using 3D geometric morphometrics. Shape differences were visualized using a principal component analysis as well as a phylogenetic principal component analysis. To assess if cranial shape differs depending on life cycle and environment, we performed phylogenetic analysis of variance (MANOVA). To assess and compare morphological disparities for each life cycle strategy (biphasic, paedomorphic, and direct development) we calculated the Procrustes variance for each life cycle using residuals of a linear model fit, and pairwise comparisons to identify differences among groups were also performed. Calculation of evolutionary rates for whole cranial shape as well as for each cranial element and comparisons across different life cycle strategies were performed based on a Brownian motion BM model of evolution. Rates of evolution in the salamander skull were analyzed using the variable rates model. In this method, a reversible-jump Markov Chain Monte Carlo (MCMC) algorithm is used to detect shifts in rates of continuous trait evolution. Ancestral state estimations were conducted in order to compare the position of shifts in rates of morphological evolution to the acquisitions of the different life cycles in Caudata. In order to test if the species with a complex life cycle (with changes in diet and environment, from an aquatic to a terrestrial environment) are more evolutionarily modular than species that have a less complex life-cycle (staying in the same environment for their whole life, such as direct developers, paedomorphic, and viviparous species), we assessed the pattern and magnitude of phenotypic modularity and integration. Next, to test if species that undergo complete metamorphosis (biphasic and direct developing species) tend to be more modular than those that encounter no or partial/ incomplete metamorphosis (paedomorphic species), we also assessed pattern and magnitude of cranial modularity. Cranial modularity was estimated using two methods developed for testing the degree of morphological integration with high dimensional data. The first method is a maximum-likelihood approach which calculates Akaike information criterion (AIC) values to assess the best supported model of modularity based on trait correlations. The second method used is covariance ratio (CR) analysis which assesses the covariances within and among hypothesized modules and compares this ratio to a null hypothesis of random assignment of shape variables to partitions.

### Research sample

152 specimens belonging to 148 species and representing all the families of Caudata were sampled for this study.

### Sampling strategy

This sample was non-random and selected in order to represent the diversity of developmental life cycles within each family as fully

### Data collection

One hundred and seven scans were generated for this study (107 species), and 45 were collected from different online repositories (data were collected by A-CF, CB, ELS and DCB). The following CT-scanners were used to scan specimens at high resolution: a Phoenix VTx L240-180 CT scanner (General Electric, Boston, MA, U.S.A.) at the X-ray tomography facility at the Museum National d'Histoire Naturelle (AST-RX platform, UMS 2700), a Phoenix nanotom X-ray|s at the Museum für Naturkunde; a Phoenix VTome|x M240 at the University of Florida's Nanoscale Research facility and made available on MorphoSource ([morphosource.org](https://morphosource.org)); a Nikon Metrology HMX ST 225 CT scanner at the CT facility of the Natural History Museum. Specimens collected from DigiMorph ([digimorph.org](https://digimorph.org)) were scanned using an ACTIS scanner at the High-Resolution X-ray Computed Tomography Facility at the University of Texas at Austin. Segmentation and exportation of the skull reconstructions of each specimen as PLY files were performed by A-CF, CB and JB. All the PLY files were imported into Geomagic Wrap (3D Systems, Rock Hill, South Carolina, USA) in order to clean, repair and decimate the meshes prior to the landmarking procedure by A-CF. Collection of the landmark was performed by A-CF.

### Timing and spatial scale

Museum specimens were scanned over the years 2016, 2017 and 2018 during at least four visits to the spirit collections of herpetology of the National History Museum (London, UK), the Museum National d'Histoire Naturelle (Paris, France) and the

Museum für Naturkunde (Berlin, Germany).

Data exclusions

Reproducibility https://github.com/anjoswami/salamanders). All the analyses were perform using different R packages and other open software (Bayestrait, BEAST)."/>

Randomization

Blinding

Did the study involve field work?  Yes  No

## Reporting for specific materials, systems and methods

We require information from authors about some types of materials, experimental systems and methods used in many studies. Here, indicate whether each material, system or method listed is relevant to your study. If you are not sure if a list item applies to your research, read the appropriate section before selecting a response.

### Materials & experimental systems

n/a	Involvement in the study
<input checked="" type="checkbox"/>	<input type="checkbox"/> Antibodies
<input checked="" type="checkbox"/>	<input type="checkbox"/> Eukaryotic cell lines
<input checked="" type="checkbox"/>	<input type="checkbox"/> Palaeontology and archaeology
<input checked="" type="checkbox"/>	<input type="checkbox"/> Animals and other organisms
<input checked="" type="checkbox"/>	<input type="checkbox"/> Human research participants
<input checked="" type="checkbox"/>	<input type="checkbox"/> Clinical data
<input checked="" type="checkbox"/>	<input type="checkbox"/> Dual use research of concern

### Methods

n/a	Involvement in the study
<input checked="" type="checkbox"/>	<input type="checkbox"/> ChIP-seq
<input checked="" type="checkbox"/>	<input type="checkbox"/> Flow cytometry
<input checked="" type="checkbox"/>	<input type="checkbox"/> MRI-based neuroimaging